BOREAS An international journal of Quaternary research

Obliquity-driven mountain permafrost-related fluvial magnetic susceptibility cycles in the Quaternary mid-latitude long-term (2.5 Ma) fluvial Maros Fan in the Pannonian Basin

ZOLTÁN PÜSPÖKI, PHILIP L. GIBBARD, LÁSZLÓ FERENC KISS, RICHARD W. MCINTOSH, EDIT THAMÓ-BOZSÓ, ZITA KRASSAY, BÁLINT SZAPPANOS, VERA MAIGUT, PÉTER KOVÁCS, DOMINIK KARÁCSONY, FERENC STERCEL, FERENC VISNOVITZ, KRISZTINA DEMÉNY, LÁSZLÓ BERECZKI, TEODÓRA SZŐCS, ÁGNES ROTÁR-SZALKAI AND TAMÁS FANCSIK

BOREAS

Püspöki, Z., Gibbard, P. L., Kiss, L. F., McIntosh, R. W., Thamó-Bozsó, E., Krassay, Z., Szappanos, B., Maigut, V., Kovács, P., Karácsony, D., Stercel, F., Visnovitz, F., Demény, K., Bereczki, L., Szőcs, T., Rotár-Szalkai, Á. & Fancsik, T. 2023 (July): Obliquity-driven mountain permafrost-related fluvial magnetic susceptibility cycles in the Quaternary mid-latitude long-term (2.5 Ma) fluvial Maros Fan in the Pannonian Basin. *Boreas*, Vol. 52, pp. 402–426. https://doi.org/10.1111/bor.12618, ISSN 0300-9483.

Magnetic susceptibility (MS) of the Quaternary long-term mid-latitude Maros fluvial fan (Pannonian Basin) was recorded to understand the stratigraphical features of source-proximal fluvial depositional settings. Three fully cored 500-m-deep boreholes were sampled at 0.5-m intervals; low-field and frequency dependent MS were measured, and complementary hysteresis and SEM-EDAX investigations were performed on selected samples. Logged susceptibility data were also used to log correlations established by a simultaneous comparison of wireline log and laboratory measurements. Time-series analyses of the susceptibility records reveal a ~41-ka and ~100-ka cyclicity. Towards the source-distal sections the intensity of the ~41-ka cycles decreases, while that of the ~100-ka cycles remains strong. Stratigraphical and spectral similarities were observed between the Maros fluvial fan and Chinese loess records; however, based on complementary magnetic data, the magnetic phase of the Maros Fan sections is related to the detrital magnetite that originates from the catchment during early postglacial permafrost degradations. The amplification of the ~41-ka cycles can be attributed to the very high susceptibility values in source-proximal settings and to the special stratigraphical feature of the distributive fluvial systems. This comprises the increased avulsion frequency on the fluvial fans in 'glacial recession periods', in concert with the 'early postglacial' occurrence of the permafrost-related magnetite originating from the catchment. As a local phenomenon, this is significant since it records the obliquity-driven variations in permafrost development in a catchment. However, fluvial and alluvial fans are widespread depositional landforms within the Eurasian mountain range and were possibly the same during the Quaternary deglaciations. Thus, obliquity-driven magnetic susceptibility variations in source-proximal fan deposits attached or adjacent to regions of loess deposition should also be considered when scanning for potential source material of aeolian deposits.

Zoltán Püspöki, Bálint Szappanos, László Bereczki, Teodóra Szőcs, Ágnes Rotár-Szalkai and Tamás Fancsik, Supervisory Authority for Regulatory Affairs, Alkotás út 50, Budapest H-1123, Hungary; Philip L. Gibbard (Corresponding author: plg1@cam.ac.uk), Scott Polar Research Institute, University of Cambridge, Lensfield Road, Cambridge CB2 1ER, UK; László Ferenc Kiss and Péter Kovács, Wigner Research Centre for Physics, Konkoly-Thege Miklós u. 29-33, Budapest H-1121, Hungary; Richard W. McIntosh, Department of Mineralogy and Geology, University of Debrecen, Egyetem tér 1, Debrecen H-4032, Hungary; Edit Thamó-Bozsó, Németh László u. 2/C, Dunakeszi H-2120, Hungary; Zita Krassay, Petőfi Lutheran Grammar School of Aszód, Régész u. 34, Aszód H-2170, Hungary; Vera Maigut, Western Balkans Green Center, Naphegy tér 8, Budapest H-1016, Hungary; Dominik Karácsony, Faculty of Earth Science and Engineering, University of Miskolc, Miskolc, Egyetemváros H-3515, Hungary; Ferenc Stercel, István út 21. IV/36, Debrecen H-4031, Hungary; Ferenc Visnovitz, Department of Geophysics and Space Science, Eötvös Lóránd University, Pázmány Péter sétány 1/c, Budapest H-1117, Hungary; Krisztina Demény, Middle-Danube-Valley Water Directorate, Rákóczi u. 41, Budapest H-1088, Hungary; *received 6th December 2022, accepted 17th April 2023.*

Alluvial and fluvial fans emanating directly from highland regions are of great importance as the initial accumulation spaces between the continuously denuded hinterlands and the fluvial successions of intra-terrestrial basins (Bull 1977; Blair & McPherson 1994; Ventra & Clarke 2018). Fluvial fans, as distributive fluvial systems, fed by extended catchments and presenting strong avulsive dynamics, are strongly controlled by variations in physical processes in the catchment and by changes in the hydraulic properties of the drainage (Hartley *et al.* 2010; Weissmann *et al.* 2010; Moscariello 2018). Consequently, they can potentially produce complex responses to climate changes (Ventra & Clarke 2018). Thus, supposing sufficiently long-term proxy records of appropriate resolution, fluvial fans may significantly contribute to Quaternary climate models (Weissmann *et al.* 2010; Harvey *et al.* 2016).

Considering the 'long-term' characteristics of such sequences, it is not a common feature. For the preservation of thick stratigraphical records, continuous tectonic subsidence is necessary (e.g. Frostrick *et al.* 1992; Harvey *et al.* 2016). However, the majority of Quaternary fluvial and alluvial fans, for example at the mouths or margins of repeatedly deglaciated valleys of mid-latitude mountains, were formed in tectonically stable or even uplifting regions (e.g. Ryder 1971; Church & Ryder 1972; Nicholls 2017;

DOI 10.1111/bor.12618

Ventra & Clarke 2018). These situations have encumbered the development of thick and long-term fluvial fan accumulations. In this respect, the Maros Fan in the Pannonian Basin (Fig. 1A, B) is a promising formation. In this area the distributary fluvial system was initially formed in the Late Miocene and continued throughout the Pleistocene, since the progressively subsiding foreland favoured the uninterrupted accumulation of the deposits.

As for the 'appropriate resolution', the fluvial feature of the fluvial fans is also challenging since the accumulation has resulted in the occurrence of frequent unconformities at the bases of channel complexes (e.g. Harvey 2012; Moscariello 2018), together with a lack of reliable geochemical proxies and of a continuous palaeontological record (Ventra & Clarke 2018). However, magnetic susceptibility as a palaeoclimate proxy emerged as a possible tool for the stratigraphical investigation of intra-terrestrial fluvial successions. Magnetic susceptibility episodes, being related to the early postglacial disintegration of mountain permafrost (Püspöki *et al*. 2016), enable the stratigraphical interpretation of thick fluvial successions, together with their correlations with globally relevant loess and marine proxy records (Püspöki *et al*. 2021b). To examine these relationships a set of fluvial settings has been investigated in the Pannonian Basin, and it is reasonable to extend the investigation to fluvial fans that are so frequent in mid-latitude mountainous regions.

In this paper the stratigraphical architecture of the Quaternary Maros Fan is presented based on wireline log correlations, completed by magnetic susceptibility logs recorded by laboratory measurements of fully cored boreholes and downhole susceptibility measurements of hydrogeological wells. The interpretation of magnetic susceptibility records is supported by complementary mineralogical and magnetic investigations. Based on the results, the stratigraphical architecture of the Maros Fan is discussed and some possible contributions of fluvial fan sequences to the terrestrial Quaternary stratigraphy in general are raised.

Geographical and geological outline of the Maros fluvial fan

Physiographic features, morphology and drainage rearrangements

The Quaternary Maros River fluvial fan is situated in the southeastern margin of the Great Hungarian Plain. Its catchment area of 30 700 km^2 is situated in Romania, extending to the Southern and Eastern Carpathians (Fig. 1B), the latter being significantly impacted by mountain glaciations and permafrost developments multiple times during the Quaternary (Popescu *et al*. 2017).

The radial axis of the source-proximal, central fan reaches 30 km, whilst together with the distal lobes, it exceeds 50 km (Fig. 1B). A high resolution shuttle radar topography (SRTM) model indicates that the most elevated source-proximal part of the fluvial fan occurs in Romania, while the Hungarian part represents the distal lobe (Fig. 1C). This distal lobe of the fluvial fan is directly attached north and northwestward to the Quaternary fluvial successions of the Makó Trough and Körös Basins, the latter representing the reference site of the Pannonian Basin Quaternary fluvial deposits (Cooke *et al*. 1979; Nádor *et al*. 2003).

Topographic interpretations have revealed braided and meandering channel planforms (Sümeghy *et al*. 2013) on the surface of the distal fan. According to optically stimulated luminescence (OSL) ages (Fig. 1C; Kiss *et al*. 2014), the frequency of the autocyclic avulsions enabled the accumulation of open-fan deposits over the entire fan surface between 18.7 and 9.6 ka. The palaeochannels of the distal lobe pass around the Battonya Ridge high (Fig. 1C). That this has a tectonic origin is indicated by the basement topography (Fig. S1A) and by seismic data (Tari *et al*. 1999). This reflects that the relative elevation of the Battonya Ridge could have impacted the shape of channels and the spatial trend of channel and lobe switching events.

A drastic change in fan development occurred around 5.3–7.1 ka, when one of the small rivers southwest of the Battonya Ridge incised through the ridge and captured the Maros causing the abandonment of the fluvial belts in the main lobes of the distal fan. This event is also documented by OSL ages ranging between 1.6 and 5.3 ka (Kiss *et al*. 2014; Fig. 1C).

Miocene–Quaternary development of the distributary system

The location of the fan formation was the Békés Basin (Fig. S1A) (Haas *et al*. 2014), which has been subsiding since the Middle Miocene (Grow *et al*. 1994). Deposition began in the Late Miocene when a 2000-m-thick delta complex was formed in the southeastern sector of the Lake Pannon. Based on the seismic data (e.g. Mattick *et al*. 1994), beside the dominant southwestwards and southeastwards progradation, local northeastward progradation related to a local SE supply has also been detected (Csato *et al*. 2015: figs 6, 13) (Fig. S1B). This can be attributed to the antecedent of the Maros River. An

Fig. 1. Location and physiographic setting of the Maros fluvial fan. A. Geographical setting in Europe (relief artist of the European topography: Kenneth Townsend). B. High resolution SRTM model of the fluvial fan and the related catchment area. C. High resolution SRTM model (re-scaled) of the fluvial fan with the published OSL data of the near-surface channel complexes (Kiss *et al*. 2014) and the borehole sections discussed in the paper.

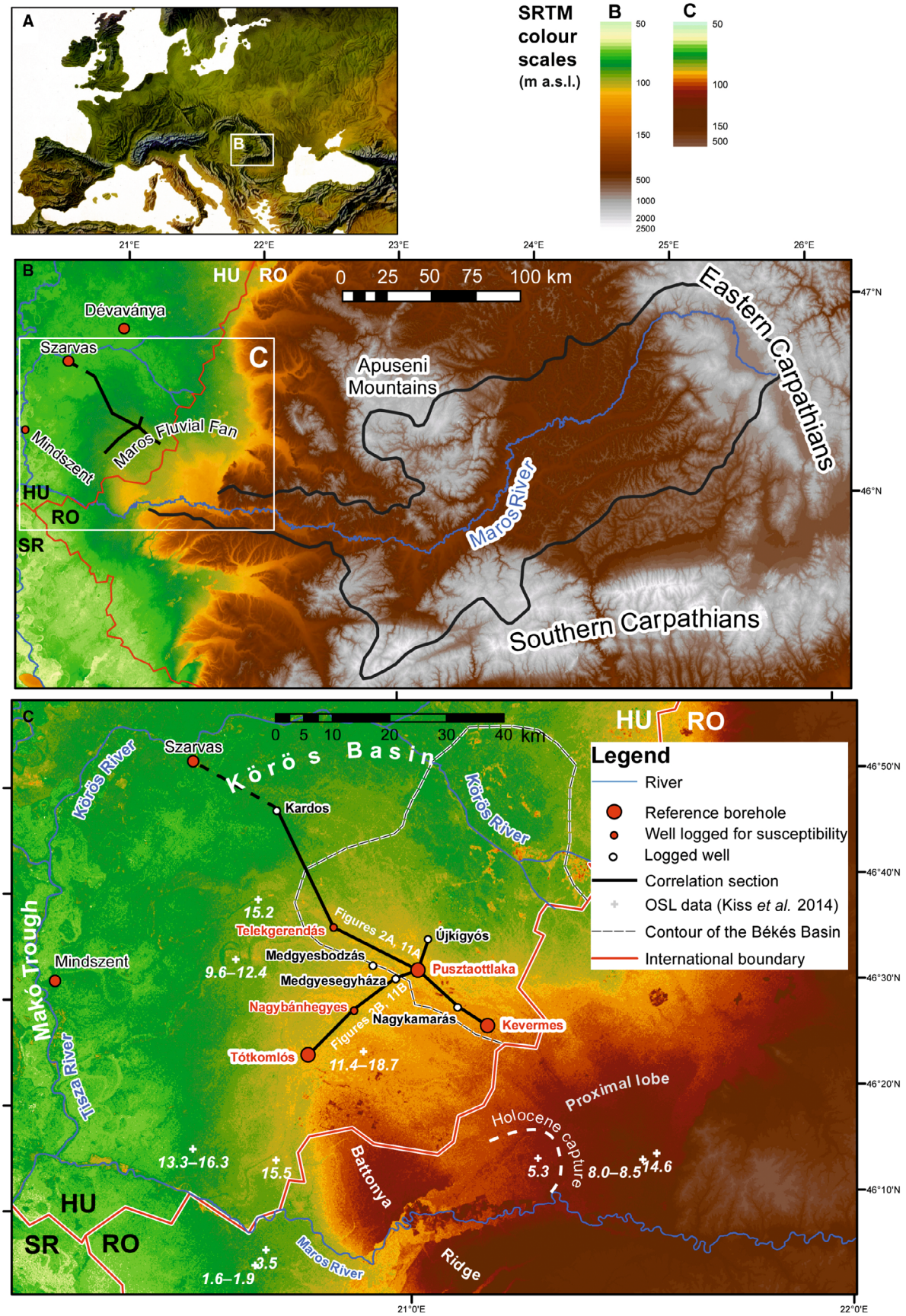

area of non-deposition was also identified above the Battonya Ridge, reflecting its Late Miocene tectonic activity.

Following the delta progradation, terrestrial fluvial fan development took place during the Pliocene and Quaternary, the deposits reaching 450–500 m in thickness. The Quaternary activity of the Battonya Ridge during the terrestrial fan development is well recorded by the seismic data, which reveal detachments ('Kunágota fault') that reach and even traverse the Quaternary strata (Fig. S1C; Koroknai *et al.* 2020; Wórum *et al.* 2020). This Quaternary fluvial fan has also been the target of geophysical and geological surveys. Three fully cored and palaeontologically investigated reference boreholes of 500 m in depth were performed (Franyó 1992) and experimental downhole geophysical investigations were undertaken (Zólyomy *et al.* 1985).

Lithology and facies characteristics of the terrestrial succession

The Maros Fan channel deposits are predominantly composed of medium-sized and coarse grey sand in the Quaternary. The sand contains a large proportion of mica, which is a special feature considered in practical sedimentological descriptions when discriminating the sediments of the Maros from those of the Tisza and Körös rivers. Gravel and gravelly sand channel deposits occur in the source-proximal upstream part of the fan in Romania.

The fan overbank deposits are dominated by silt and clay of various proportions with thin sand intercalations. The Maros Fan flood-plain deposits are also peculiar in that they include a higher proportion of silt than of clay, especially in the upper parts of the succession. There are silt layers of very low clay content, frequently interpreted as air-transported dust that accumulated in flood-plain conditions; however, this could also be interpreted as overbank silt that originated from catchment regions during deglaciation periods (cf. Weissmann *et al.* 2002).

The overall appearance of the fan succession has an explicit upward-coarsening feature in wireline logs (Fig. 2). This change is a characteristic feature of prograding fluvial fans (e.g. Weissmann *et al.* 2013). Superimposed on this upward coarsening trend is a general increase in sand that can be observed in the upper part of the Quaternary succession. This upper 100–150 m of the fan complex is dominated by thick multiple channel complexes sometimes of tens of metres in thickness, while overbank deposits are subdominant.

Biostratigraphy of the reference boreholes

As a consequence of the restricted extent of palaeomagnetic data available, biostratigraphy is indispensable in the stratigraphical correlations of the Pannonian Basin Quaternary fluvial succession. The Lower and Middle Pleistocene are characterized by a specific molluscan fauna (Kretzoi & Krolopp 1972; Krolopp 1995, 2002). The *Viviparus boeckhi* biozone is determined by the presence of *Viviparus boeckhi* Halaváts, 1888, the last appearance datum of which (LADVb) occurs within the Brunhes Epoch in magnetic susceptibility cycle III according to Püspöki *et al.* (2021b), while its first appearance datum (FADVb) coincides with the Olduvai Subchron. An additionally important chrono-species occurring in the *Viviparus boeckhi* biozone is the concurrent *Planorbis planorbis* f. *dentata* Krolopp, 1976, which can be identified based on its characteristic fragments. Furthermore, *Parafossarulus crassitesta* (Brömme, 1885), identified based on its specific opercula, became extinct at the LADVb (Krolopp 2002). The latter also occurs in the Pliocene deposits in the basin.

In the Pusztaottlaka section (Krolopp 1983a), the upper boundary of the *Viviparus boeckhi* biozone is indicated by the occurrence of *Planorbis planorbis* f. *dentata* at 100.5–101.0 m (Figs 2A, 3A). The specimens of *Viviparus boeckhi* occur only at 191.7–192.5 m depth (Figs 2A, 3B). However, the lower boundary of the *Viviparus boeckhi* biozone is much deeper, it being well represented by the occurrence of *Planorbis planorbis* f. *dentata* between 338.0–338.3 m (Figs 2A, 3C). At 440-m depth some specifically ornamented *Unio* fragments were found (Figs 2A, 3D), the age of which is ambiguous. However, in Hungarian malacology they are usually considered as an indicator of a pre-Quaternary age (Krolopp 2002). The first mollusc remnant proving unambiguously the pre-Quaternary age of the sediments unambiguously is a Dreisseninae fragment from a depth of 496 m.

In the Kevermes section (Krolopp 1983b), the upper boundary of the *Viviparus boeckhi* biozone is indicated by finds of *Planorbis planorbis* f. *dentata* fragments that occur at 133.0–133.5 m (Figs 2A, 3E). Unfortunately, the next stratigraphically relevant mollusc remnants in the Kevermes section are those of *Melanopsis* sp. and *Dreissena* sp. at 487.0–487.5 m depth (Figs 2A, 3F, G), demonstrating the pre-Quaternary age of the sediments below 487.0 m. Thus, the lower boundary of the *Viviparus boeckhi* biozone must occur between 133.5 m and the pre-Quaternary segment of the section.

In the Tótkomlós borehole (Krolopp 1982) the upper boundary of the *Viviparus boeckhi* biozone is identified based on the occurrence of *Parafossarulus crassitesta* opercula at a depth of 68.66–68.79 m (Fig. 2B). At 219.40–222.61 m the pre-Quaternary age of the sediments is indicated by finds of *Melanopsis* sp. together with the ornamented Unionidae fragments (Fig. 2B). A photographic record of this borehole was impossible because of the mixing of labels on the boxes containing the samples. This, together with the partial mixing of the specimens within the boxes, makes it uncertain to determine the precise depth and stratigraphical position of the specimens.

Nevertheless, the evidence recovered demonstrates that all three reference boreholes span the entire

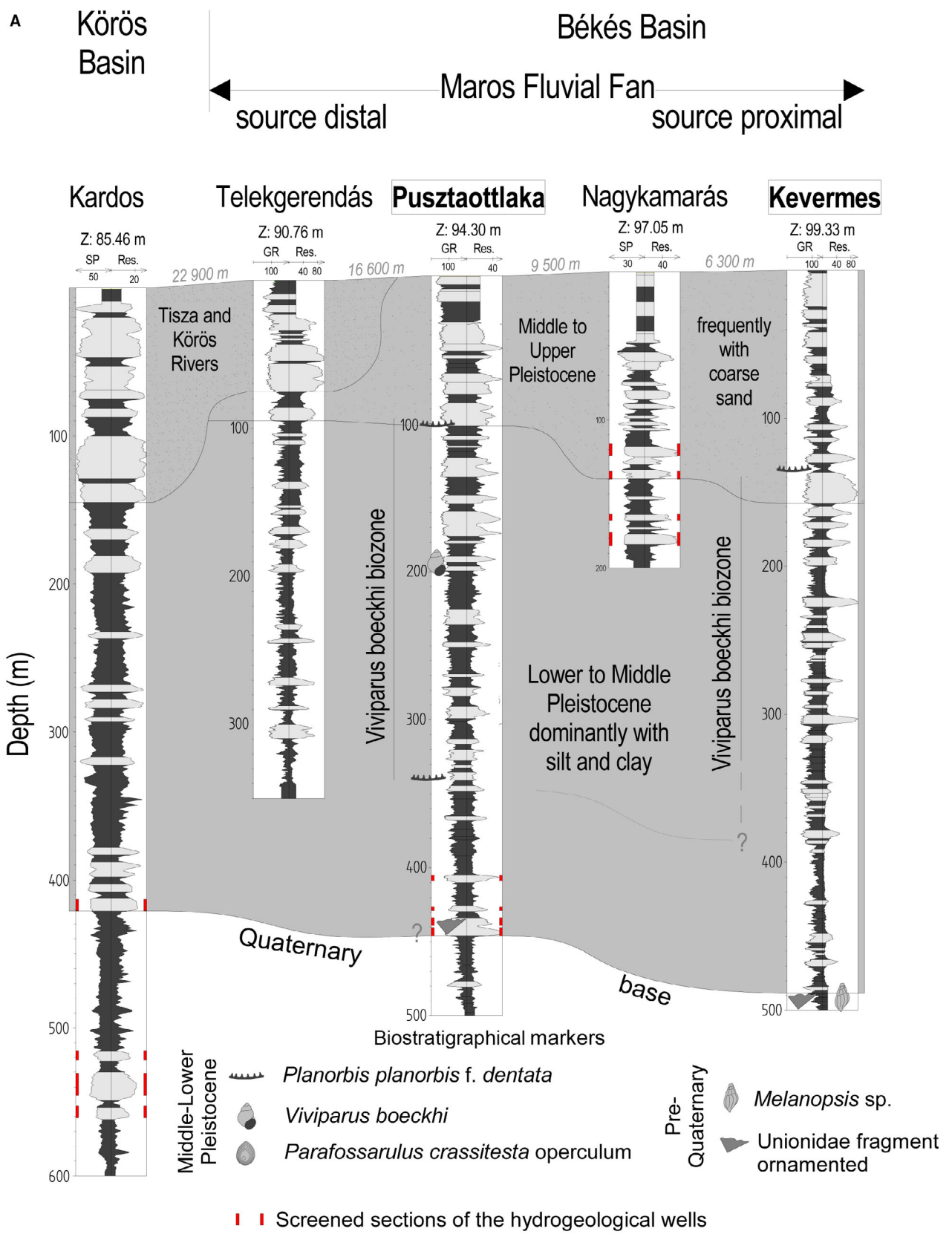

Fig. 2. Lithology, palaeontology and log facies characteristics of the Maros fluvial fan. A. Dip oriented section presenting the contact of the Békés and Körös Basins. B. Strike oriented section presenting the contact of the Békés Basin and the Battonya Ridge.

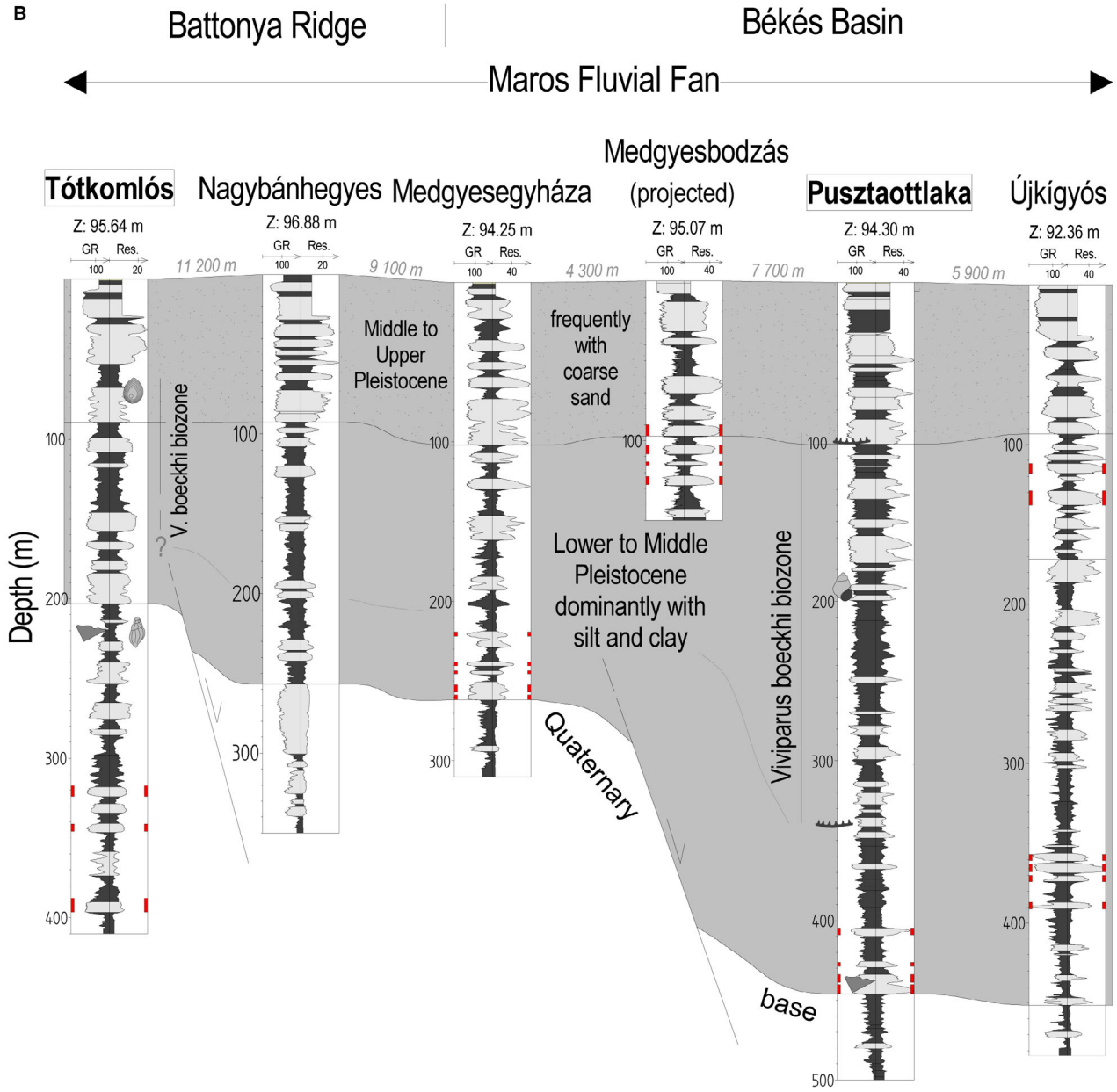

Fig. 2. (Continued)

Quaternary succession. Moreover, the lack of a palaeomagnetic age determination has been well compensated for by the regional biostratigraphical evidence, i.e. the identification of the Pleistocene *Viviparus boeckhi* biozone. The latter results proved the limited thickness of the Quaternary succession above the Battonya Ridge (Fig. 2B).

Material and methods

Low-field magnetic susceptibility (χ_{LF}) of the reference boreholes, Pusztaottlaka, Kevermes and Tótkomlós, was recorded at ~0.5-m sampling intervals (~3 ka), using the inner parts of the cores. The numbers of samples in the boreholes are $n = 864$, 861 and 735, respectively. The material was placed in plastic boxes of 2.5×2.5 cm. Measurements were made using a SI-2 susceptibility instrument operating at 750 Hz and at a peak field of 1 Oe at the laboratory of the Supervisory Authority of Regulatory Affairs (SARA). To determine the frequency dependent susceptibility (χ_{FD}%), low (470 Hz) and high (4700 Hz) frequency measurements were performed in a Bartington MS2 magnetometer. The R^2 of linear correlation between Bartington MS2 (470 Hz) and SI-2 (750 Hz) were 0.9996, 0.9998 and 0.9996 in the Pusztaottlaka, Kevermes and Tótkomlós sections, respectively.

To determine the magnetic mineralogy of the core sediments, the magnetic fractions of representative

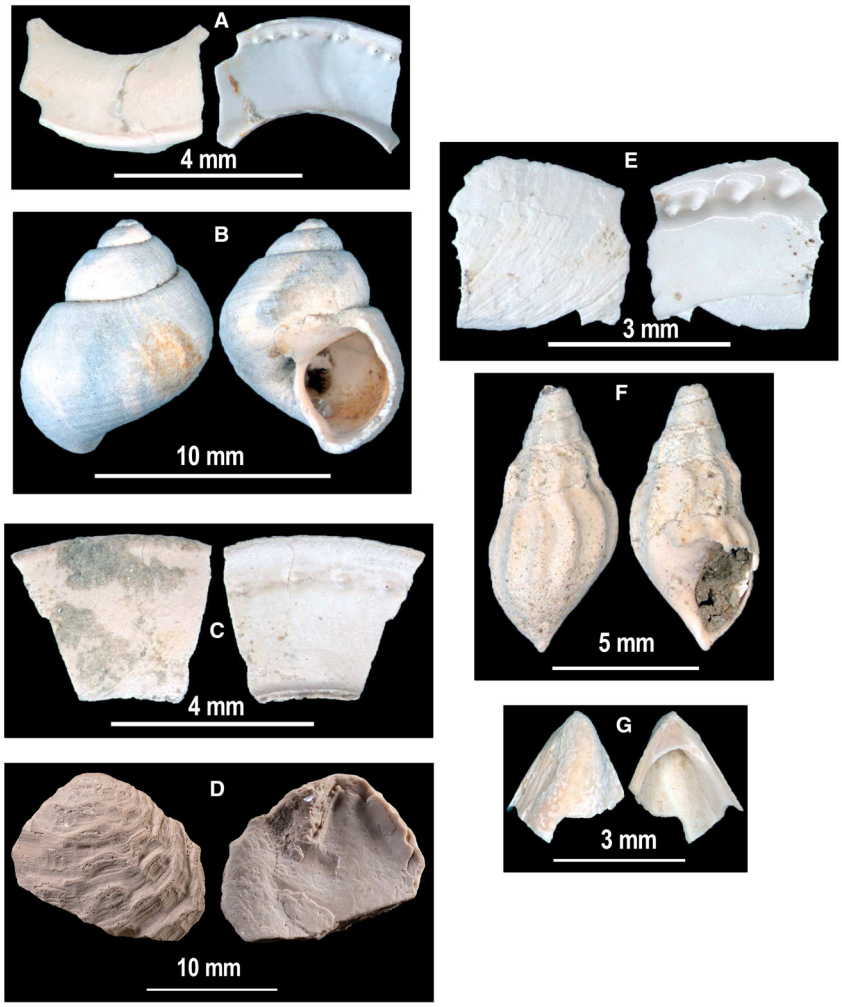

Fig. 3. Biostratigraphical markers of the reference boreholes of the Maros fluvial fan. A. *Planorbis planorbis* f. *dentata* (Pusztaottlaka 100.5–101.0 m). B. *Viviparus boeckhi* (Pusztaottlaka 191.7–192.5 m). C. *Planorbis planorbis* f. *dentata* (Pusztaottlaka 338.0–338.3 m). D. Ornamented Unionidae fragment (Pusztaottlaka 440.0 m). E. *Planorbis planorbis* f. *dentata* (Kevermes 133.0–133.5 m). F. *Melanopsis* sp. (Kevermes 487.0–487.5 m). G. *Dreissena* sp. (Kevermes 487.0–487.5 m).

samples were separated using a hand-held magnet (cf. Heider *et al*. 2001). Magnetic grains were studied using a Thermo Scientific Scios 2 dual-beam scanning electron microscope (SEM) with Shottky-cathode at 15 kV. An atomic number sensitive back-scattered electron detector was applied to show Fe containing, high contrast magnetic grains. Chemical compositions were measured using a BRUKER (SSD) energy dispersive spectrometer with ~30-s detection time and ~8000–10 000 cps.

To perform quantitative evaluation of the magnetic minerals, hysteresis curves of selected sample sets were measured at room temperature (T = 300 K) in a SQUID magnetometer (Quantum Design MPMS-5S) in the magnetic-field range of $\pm H$ = 50 kOe. Temperature dependence of the magnetic moment of the samples with the highest magnetite content was measured using a small magnetic field (H = 10 Oe) between 5 and 300 K both in ZFC (zero-field cooling) and in FC (field cooling) modes. In ZFC mode, the samples were cooled from 300 to 5 K in zero field and the magnetic moments of the samples were measured in the measuring field during warming. In FC mode, the samples were cooled in the measuring field from 300 to 5 K before measuring their magnetic moment at the same field during warming.

In the time-series analysis, the re-scaling of the magnetic susceptibility records was performed by piecewise linear interpolation, using AnalySeries (Paillard *et al*. 1996). The spectral estimations were made by the multi-taper method (MTM; Thomson 1982, 1990), which enables investigation of the statistical significance. The data were linearly detrended and pre-whitened; the number of tapers was six. Evaluating the statistical significance of spectral peaks, the spectral background was approximated with the quadratic fit of the log power vs. frequency data; the degrees of freedom were considered to be 12, i.e. twice the number of tapers (Weedon 2003). The fundamental Milankovitch frequencies i.e. eccentricity, obliquity and precession for the last 2.5 Ma were used according to the analytical

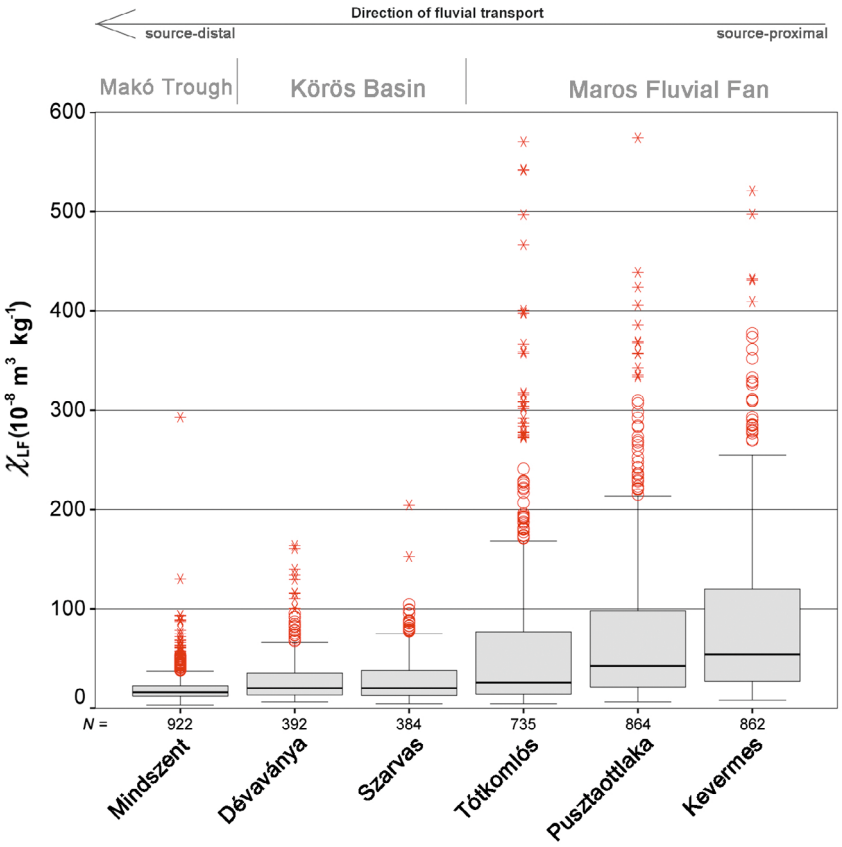

Fig. 4. Box plots of the low-field magnetic susceptibility values of the Maros fluvial fan and the neighbouring basin settings (Körös Basin, Makó Trough) based on laboratory measurements.

solution by Laskar *et al.* (2004) and expressed spectrally also by MTM.

A continuous wavelet transformation was also performed to examine the temporal evolution of the re-scaled susceptibility records (Foufoula-Georgiou & Kumar 1994). Morlet mother wavelet was applied with free frequency parameter of a relatively high value, thus enabling investigation of the time/period distribution of the signal's energy with good spectral period resolution. In scalograms coloured according to the logarithms of the wavelet coefficients of the time/period domains, the cone of influence and the 95% confidence level of a red-noise process (Torrence & Compo 1998) are indicated. Wavelet spectra of the signals, as the period dependent averages of the wavelet coefficients computed over time, were also calculated.

Results

Spatial variation of magnetic susceptibility values

The exploration data analysis (EDA) of the laboratory measurements (Fig. 4) revealed that the low-field magnetic susceptibility of the fluvial materials deposited on the surface of the source-proximal Maros Fan is significantly higher than that of those transported towards the source-distal settings of the Körös Basin and Makó Trough. Practically the interval of the stratigraphically significant outlier and extreme values ranging between 80× and 200×10^{-8} m^3 kg^{-1} in the Körös Basin overlap with the interval representing the upper quartile of the Maros Fan sections. At the same time the outlier and extreme values occurring in the Maros Fan are unique in their high values in the Pannonian Basin. This is the reason why hereafter, in the log correlation sections of the Maros Fan, the upper quartile (Q3) range is also highlighted by a red colour together with the outlier and extreme values (Fig. 5).

Stratigraphical correlation of magnetic susceptibility records

Laboratory measured low-field susceptibility (χ_{LF}) values of the reference boreholes are plotted together with Dévaványa and Szarvas as reference sites representing the Pannonian fluvial succession (Püspöki *et al.* 2021b) (Fig. 5) and the Jingbian section (Ding *et al.* 2005) representing the Chinese loess sequences. The labelling of χ_{LF} maxima and susceptibility cycles is according to Püspöki *et al.* (2021b).

An apparent feature of the sections is the existence of extremes (MP10, 10a) at the base of the Quaternary

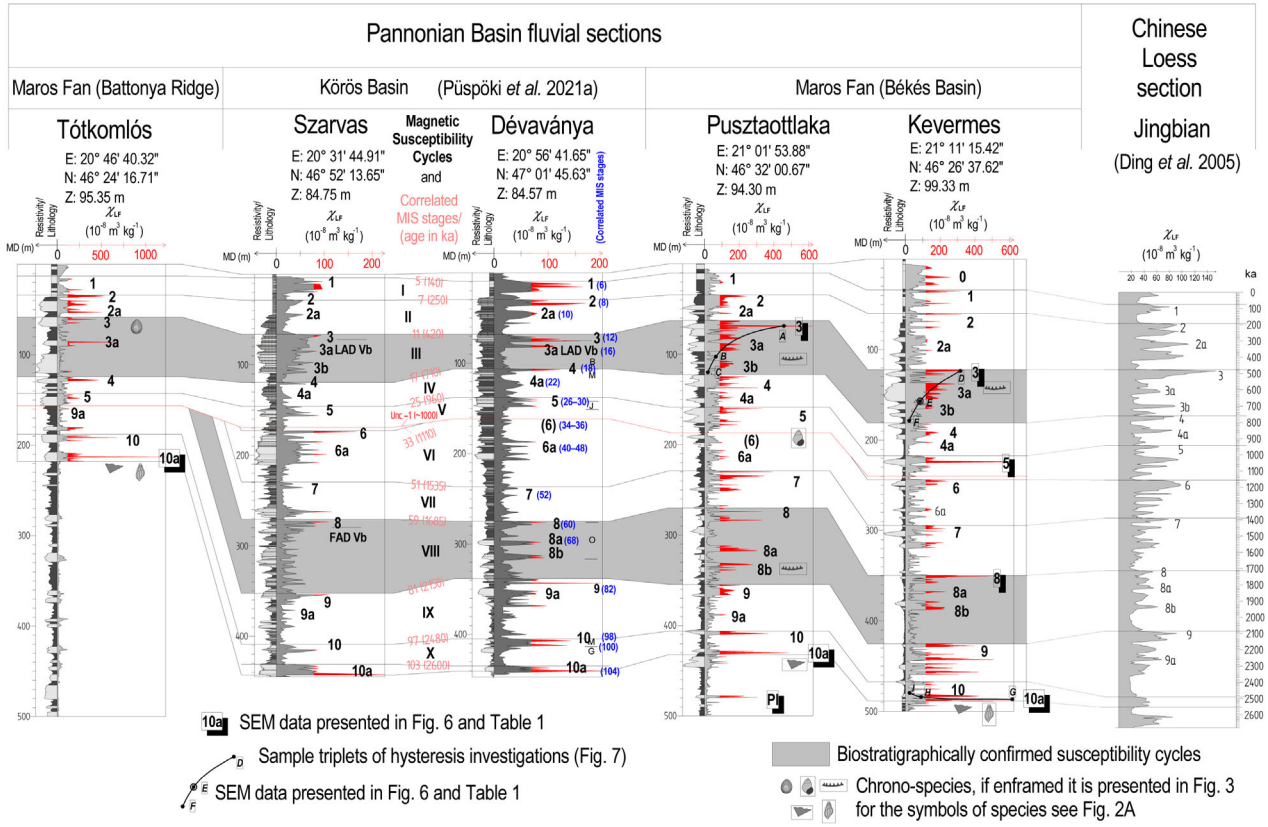

Fig. 5. Stratigraphical correlation of low-field magnetic susceptibility records of the reference boreholes of the Maros fluvial fan based on laboratory measurements in comparison with the reference sections in the Körös Basin (Püspöki *et al.* 2021b) and in the Chinese Loess Plateau (Ding *et al.* 2005). The upper quartile (Q3) range together with the outlier and extreme values are highlighted by red colour in χ_{LF} tracks.

succession, which is confirmed by palaeomagnetic data in the Dévaványa section and by the occurrence of pre-Quaternary molluscs in the Maros Fan sections. Another similarity is the existence of the MP9 9a and MP8 8a, 8b maxima both in the Körös Basin and in the Maros Fan–Békés Basin sections. These peaks can also be correlated with peaks in the Jingbian section. The upward-increasing nature of susceptibility cycle IX is very similar in the Dévaványa, Szarvas and Pusztaottlaka sequences.

As a special feature, MP7 and MP6 can be detected in the Maros Fan sections; the former is especially clearly expressed in Pusztaottlaka, the latter in Kevermes. The appearances of χ_{LF} maxima in susceptibility cycles VII and VI are more similar to the Chinese loess section than to those of the neighbouring Körös Basin. The lack of MP6 in the Dévaványa and Pusztaottlaka boreholes can be explained as a result of the Regional Unconformity-1 of ~1000 ka (cf. Püspöki *et al.* 2021b), which is a correlative conformity in the Szarvas and Kevermes sections containing MP6.

From MP5 up to the MP3, which is confirmed by palaeontology, the correlation is also reliable. Two specific features of the Maros Fan sections are: (i) the extreme MS maxima of MP5 in Kevermes, and (ii) the explicit upward-increasing nature of susceptibility cycle III containing 3b, 3a and MP3 χ_{LF} maxima in the Maros Fan sections. The appearance of susceptibility cycle III is also more similar to that in the Chinese loess section than to that in the Körös Basin.

The uppermost MP2, MP1 and MP0 peaks indicate that the Kevermes section is more complete than that at Pusztaottlaka. This is presumably a result of the more intensive subsidence at Kevermes, which occurs closer to the centre of the Békés Basin. This subsidence may explain the preservation of MP6 in the Kevermes section whilst it is so rare in the Pannonian sections.

The Tótkomlós section represents the Maros Fan sequence in the area of the Battonya Ridge. Considering the limited thickness of the Quaternary succession here and the limited number of χ_{LF} maxima, the Tótkomlós section is rather incomplete. The strongly correlated peaks are: (i) the palaeontologically confirmed MP3, and the very extreme MP10a. The value of the MP10a χ_{LF} peak is $>1300 \times 10^{-8}$ m^3 kg^{-1} (!) in Tótkomlós and $>2000 \times 10^{-8}$ m^3 kg^{-1} (!) in Kevermes, which is entirely unique up to the present in the Pannonian Basin fluvial Quaternary. This can be considered a specific feature of the Quaternary base in the Maros fluvial fan, supporting

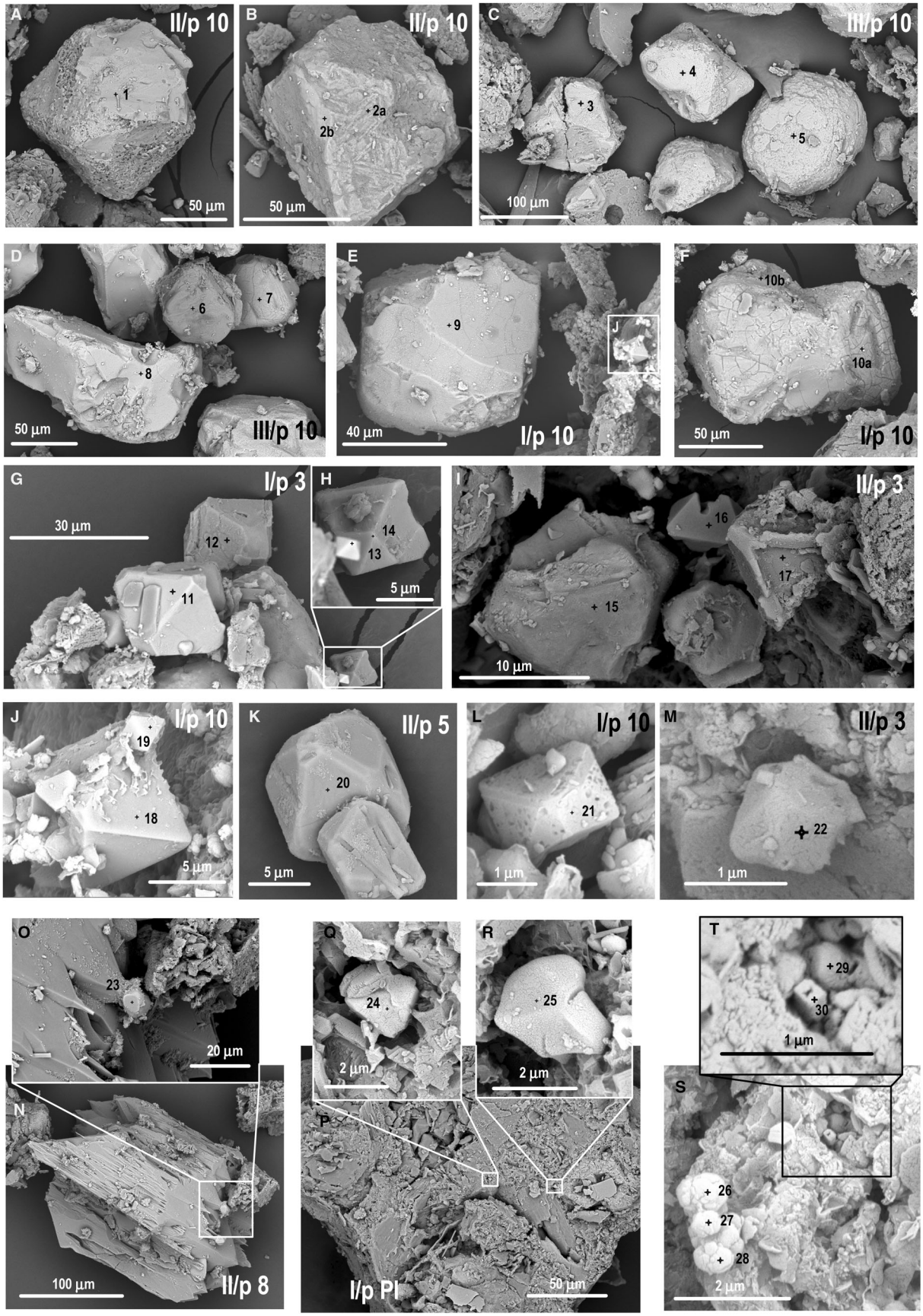

Fig. 6. SEM images of the magnetic fraction separated from representative susceptibility maxima of the reference boreholes. A. Idiomorphic magnetite octahedron of >100 μm from MP10 of Kevermes section (487.00 m). B. Idiomorphic magnetite octahedron of >100 μm with exsolution structures from MP10 of Kevermes section (487.00 m). C. Magnetic grains of ~100 μm from MP10 of Tótkomlós section (213.00 m), the large, rounded grain (measured point 5) is either titanomagnetite or ilmenite based on its high titanium content. D. Magnetic grains of 50–100 μm from MP10 of Tótkomlós section (213.00 m). E. Idiomorphic magnetite octahedron of ~50 μm from MP10 of Pusztaottlaka section (430.00 m). F. Intergrown idiomorphic magnetite octahedrons of ~50 μm from MP10 of Pusztaottlaka section (430.00 m). G. Idiomorphic magnetite octahedrons of ~20 μm from MP3 of Pusztaottlaka section (72.00 m). H. Idiomorphic magnetite octahedrons of 2–10 μm from MP3 of Pusztaottlaka section (72.00 m). I. Idiomorphic magnetite octahedrons of 5–15 μm from MP3 of Kevermes section (123.50 m). J. Idiomorphic magnetite octahedrons of 2–10 μm from MP10 of Pusztaottlaka section (430.00 m). K. Idiomorphic magnetite octahedron of ~10 μm from MP5 of Kevermes section (224.00 m). L. Idiomorphic magnetite octahedrons of ~2 μm from MP10 of Pusztaottlaka section (430.00 m). M. Idiomorphic magnetite octahedrons of ~1 μm from MP3 of Kevermes section (123.50 m). N. Pyroxene (hypersthene) crystal with small magnetic inclusions from MP8 of Kevermes section (351.00 m). O. Idiomorphic magnetite octahedron of <10 μm as an inclusion in a large pyroxene crystal from MP8 of Kevermes section (351.00 m). P. Large silica fragment with small magnetic grains as inclusions from the Pliocene susceptibility maximum of Pusztaottlaka section (479.50 m). Q. and R. Idiomorphic magnetite octahedrons of ~2 μm as inclusions in a large silica fragment from the Pliocene susceptibility maximum of Pusztaottlaka section (479.50 m). S. Ferrium-sulphide aggregates of <1 μm in the magnetic fraction of a sample with outlying coercivity (Kevermes 157.00 m). T. Idiomorphic magnetite octahedrons of <0.5 μm in the sample with outlying coercivity.

at the same time the identification of MP10a in the incomplete Tótkomlós section. The lack of MP6–MP9 χ_{LF} peaks at Tótkomlós can be attributed to the Regional Unconformity-1 at ~1000 ka.

In summary, the magnetic susceptibility records of the Maros Fan can be correlated with the nearby Dévaványa section of magnetostratigraphical constraints. Nevertheless, the Maros Fan sections have some special features that differ from the Dévaványa section and are somewhat more similar to those in the Chinese loess section.

Magnetic granulometry

Frequency dependent susceptibility (χ_{FD}%) measurements were performed to investigate the superparamagnetic nature of the susceptibility maxima (cf. Zhou *et al.* 1990). The measurement conditions allowed reliable measurements above $\sim 60 \times 10^{-8}$ m^3 kg^{-1}. Since the stratigraphically relevant χ_{LF} values in the sections are above $\sim 100 \times 10^{-8}$ m^3 kg^{-1}, this sensitivity enabled the reliable measurement of all the relevant samples. The χ_{FD}% of samples ranges between 0 and 5% independently of the χ_{LF} (Fig. S2A). Based on published models (Dearing *et al.* 1996), this value of χ_{FD}% indicates a subdominant proportion of superparamagnetic grains. To check the reliability of the especially high value of MP10a in Kevermes ($>2000 \times 10^{-8}$ m^3 kg^{-1}) this interval was re-sampled at 10-cm intervals, which enabled a detailed comparison of χ_{LF} and χ_{FD}%, confirming the independence of the two parameters (Fig. S2B).

To investigate the superparamagnetic fraction by an alternative method, the temperature dependence of the magnetic moment was measured in a small field (10 Oe) on the sample MP10a in the Kevermes section at a depth of 487.00 m in ZFC and FC modes. It is well documented that in a superparamagnetic particle system in ZFC mode the susceptibility should increase as the particles unblock in a 10 Oe warming field and should decrease for higher temperatures according to Curie's law (e.g. Dormann *et al.* 1997; Kosterov 2001, 2003; Knobel *et al.* 2008).

Although the behaviour of the ZFC and FC curves at low temperatures resembles that of a superparamagnetic (SPM) particle assembly (Fig. S2C), the constant value of the magnetic moment at high temperatures suggests that the majority of the sample is in a FM multidomain state. Therefore, only a small proportion of the magnetite might be in an SPM state. The abrupt increase of the magnetic moment with decreasing temperature could mean that some of these SPM particles are so small in size that their blocking temperatures are below the lowest temperature of the measurements ($T = 5$ K).

Therefore, the magnetic phase of the Maros Fan sections is predominantly not superparamagnetic. Thus, a climate-dependent variation of the detrital magnetic phase can be assumed.

Mineralogy of the ferromagnetic fraction

To characterize the magnetic mineralogy, the magnetic phase was separated from samples representing the regionally correlated peaks MP3 and MP10 from the reference boreholes, and MP5 and MP8 from the Kevermes borehole. Based on SEM-EDAX investigations (Fig. 6, Table 1), the magnetic phase is dominated by the presence of detrital magnetite of various origins and grain sizes. Slightly rounded idiomorphic octahedrons of 50–100 μm make up a significant proportion of the magnetite grains (Fig. 6A–F, measured points 1–10). Sometimes traces of exsolution (Fig. 6B) and occurrence of intergrown octahedrons (Fig. 6F) can also be detected. Among the magnetite octahedrons, fractions of larger magnetic grains without characteristic crystal forms can also be found (measured points 5 and 8).

Besides the 50–100 μm rounded octahedrons, well-shaped small octahedrons with diameters ranging from 2 to 20 μm can also be detected in the samples (Fig. 6G–M, measured points 11–22). The better preservation of the small fraction can be attributed to its transport mechanism since the 2–20 μm fraction is mostly transported in suspension, while the 50–100 μm fraction is moved by saltation.

A high proportion of silicate grains can occur in the separated magnetic fraction, indicating their magnetite inclusions. Pyroxene (hypersthene) crystals, presumably of volcanic origin (Fig. 6N), contain magnetite

Table 1. Chemical composition (mass percent) of the selected magnetic particles (for the space and form of the grains see Fig. 6).

Mp	Section	Depth (m)	Stratigraphy	C	O	Na	Mg	Al	Si	S	K	Ca	Ti	Fe	Mn	Au	Size (μm)	Maintenance	Photo (Fig. 6)
1	Kevermes	487	MP10	4.56	35.15	0.09	0.99	4.4	4.42				5.35	40.81		4.23	>100	Idiomorphic	A
2a	Kevermes	487	MP10	0.89	8.44	0	0	3.94	4.6				11.13	64.13		6.88	~100	Idiomorphic	B
2b	Kevermes	487	MP10	0.6	6.86	0	0	3.75	4.44				12.15	65.65		6.54	~100	Idiomorphic	B
3	Tótkomlós	213	MP10	4.8	31.51		0.39	0.96	1.33				15.67	39.09		6.24	~100	Idiomorphic	C
4	Tótkomlós	213	MP10	5.11	15.66		0.72	1.62	1.49				9.5	55.15		10.75	~100	Idiomorphic	C
5	Tótkomlós	213	MP10	2.74	10.47		1.55	2.11	3.97				31.44	35.53		12.2	>100	Rounded	C
6	Tótkomlós	213	MP10	0.51	37.56			1.26	1.45				5.52	52.94		0.77	~50	Idiomorphic	D
7	Tótkomlós	213	MP10	2.77	19.1		2.24	2.75	1.44				13.2	53.69		4.82	~50	Idiomorphic	D
8	Tótkomlós	213	MP10	6.12	36.53	0.34	0.39	0.97	1.25				3.45	44.48		6.47	>100	Fragment	D
9	Pusztaottlaka	430	MP10	3.55	37.92	0.58	0.91	3.14	4.99				8.05	36.11	1.63	2.86	~50	Idiomorphic	E
10a	Pusztaottlaka	430	MP10	4.02	43.7			1.98	3.82				1.65	42.93		1.9	>50	Idiomorphic	F
10b	Pusztaottlaka	430	MP10	2.8	27.11	0.55	0.59	2.29	4.36				2.98	54.19		5.13	>50	Idiomorphic	F
11	Pusztaottlaka	72	MP3	4.16	24.35	0.24	1.39	2.11	2.2				10.47	48.34		6.73	~20	Idiomorphic	G
12	Pusztaottlaka	72	MP3	3.96	12.51	0.98	0.99	3.21	7.7				16.19	51.48		2.95	~20	Idiomorphic	G
13	Pusztaottlaka	72	MP3	9.85	28.52	0.43	1.38	5.73	5.07				8.28	37.5		3.24	~2	Idiomorphic	G/H
14	Pusztaottlaka	72	MP3	3.42	22.71	0.1	0.95	1.98	1.12				12.24	50.62		6.86	~10	Idiomorphic	G/H
15	Kevermes	123.5	MP3	2.31	16.16	0.51	0.38	2.12	3.67				27.14	39.68		8.04	>20	Fragment	I
16	Kevermes	123.5	MP3	0	0	0.1	0.25	0	0				20.67	76.68		2.3	~5	Idiomorphic	I
17	Kevermes	123.5	MP3	0	2.31	0	0	1.14	4.54				19.98	67.67		4.33	~10	Idiomorphic	I
18	Pusztaottlaka	430	MP10	2.8	27.11	0.55	0.59	2.29	4.36				2.98	54.19		5.13	~10	Idiomorphic	J
19	Pusztaottlaka	430	MP10	2.99	29.87	0.76	2.61	2.66	5.04				19.61	30.74		5.73	~2	Idiomorphic	J
20	Kevermes	224	MP5	5.32	26.44	0.49	0.5	1.81	2.8				10.34	48.22		4.08	~10	Idiomorphic	K
21	Pusztaottlaka	430	MP10	5.25	33.92	1.19	1.19	2.22	3.51				9.25	38.24		5.97	~2	Idiomorphic	L
22	Kevermes	123.5	MP3	4.6	31.51	0.23	1.4	2.28	3.07				6.12	45.19		5.59	~1	Idiomorphic	M
23	Kevermes	351	MP8	1.58	9.61		5.81	3.81	8.37				7.09	54.99		8.75	<10	Inclusion	N/O
24	Pusztaottlaka	479.5	Pliocene	0.62	16.92	0.57		1.66	3.25				10.9	57.6		8.14	~2	Inclusion	P/Q
25	Pusztaottlaka	479.5	Pliocene	0	22.86	0	1.16	2.53	4.51				10.36	53.28		5.29	~2	Inclusion	P/R
26	Kevermes	157	small MS	7.71	24.94		0.33	1.45	3.52	17	0.28	1.23	0	35.01		8.5	<1	Aggregate	S
27	Kevermes	157	small MS	6.25	29.89			1.17	3.06	15		1.23	0	35.34		8.03	<1	Aggregate	S
28	Kevermes	157	small MS	5.52	27.03			0.74	2.2	22		0.91	0.01	38.18		3.38	<1	Aggregate	S
29	Kevermes	157	small MS	1.96	33.65			1.62	3.59	2.11		1.33	0	50.67		5.07	<0.5	Idiomorphic	T
30	Kevermes	157	small MS	1.23	29.64		0.19	1.4	3.42	1.77	0.17	1.31	0	58.19		2.68	<0.5	Idiomorphic	T

Table 2. Parameters deduced from the hysteresis curves for the nine selected samples (χ^{PM} and ρ^{PM} are susceptibility and density of sand, respectively, c^{FM} and c_v^{FM} are mass and volume concentration of magnetite, respectively, and H_c is coercive field).

Sample	χ^{PM} (10^{-6} emu g^{-1} Oe^{-1} or 10^{-8} m^3 kg^{-1})	ρ^{PM} (g cm^{-3})	c^{FM} (w.%)	(v.%)	H_c (Oe)
Pusztaottlaka 69.00 m	3.88/4.88	0.974	0.307	0.0573	40
Pusztaottlaka 103.50 m	5.27/6.62	0.798	0.0862	0.0131	45
Pusztaottlaka 120.00 m	7.08/8.90	0.883	0.011	0.00184	95
Kevermes 123.50 m	3.01/3.78	0.87	0.107	0.0177	60
Kevermes 157.00 m	6.25/7.85	0.804	0.165	0.0253	280
Kevermes 180.50 m	6.79/8.53	0.931	0.00809	0.00143	70
Kevermes 479.00 m	6.77/8.51	0.96	0.013	0.00239	45
Kevermes 484.50 m	8.40/10.6	0.843	0.0737	0.0119	50
Kevermes 487.00 m	5.08/6.38	0.878	1.2	0.202	30

octahedrons with diameters less than 10 µm (Fig. 6O, measured point 23). They become visible as a result of a degree of dissolution of the host mineral. Large silicate grains (Fig. 6P) frequently contain magnetite inclusions hardly reaching 2 µm (Fig. 6Q, R, measured points 24, 25). These small magnetite inclusions may also be a source of the 2–20 µm magnetite fraction, escaping from the enclosing silica mineral in the course of transportation.

In close correspondence to SEM investigations, the temperature dependence of the magnetic moment of the Kevermes sample from 487.00 m (Fig. S2C) showing a breaking point at around $T = 120$ K in the ZFC curve might hint at the Verwey temperature, which is a characteristic feature of magnetite (Walz 2002). However, the same feature can hardly be seen in the FC curve, which can be interpreted as the result of some degree of oxidation or cation substitution (cf. Muxworthy & McClelland 2008; Özdemir & Dunlop 2010).

The ferri- and paramagnetic contents and their relationship to magnetic susceptibility

To determine the contribution of ferri- and paramagnetic fractions to the χ_{LF} values, hysteresis investigations were performed following the standard method (e.g. Dunlop & Özdemir 1997; Leonhardt 2006; Paterson *et al.* 2018) used also in the case of Quaternary sediments (e.g. Deng *et al.* 2004; Zan *et al.* 2010; Chen *et al.* 2012). The investigated samples represent the entire range of the measured χ_{LF} values (Fig. 5).

The magnetization of a given sample as a function of the magnetic field, M (H), is described over $|H| = 20$ kOe by the sum of the paramagnetic (PM) and the ferrimagnetic (FM) contribution (Cullity & Graham 2009):

$$M = \left(1-c^{FM}\right)\chi^{PM}\,H + c^{FM}\,M^{FM}(H), \qquad (1)$$

where $c^{FM} = w^{FM}/w$ is the weight (mass) ratio of the FM component, the sample mass (w) is the sum of the mass of the PM (w^{PM}) and FM (w^{FM}) components, χ^{PM} and M^{FM} are the mass susceptibility of the PM and the saturation magnetization of the FM component, respectively. Since the dia- and paramagnetic fractions cannot be separated from each other, in fact χ^{PM} is the sum of the diamagnetic and paramagnetic susceptibility where the paramagnetic component prevails. Based on the SEM-EDAX data, the FM component is considered to be magnetite with $M^{FM} = 92$ emu g^{-1}, 92 Am^2 kg^{-1} (Cullity & Graham 2009).

The volume ratio of the FM component (c_v^{FM}) is expressed as

$$c_v^{FM} = \frac{1}{1 + \left(\frac{w}{w^{FM}} - 1\right)\frac{\rho^{FM}}{\rho^{PM}}}, \qquad (2)$$

where the sample volume (V) is the sum of the PM (V^{PM}) and FM (V^{FM}) components, ρ^{PM} (0.8–1 g cm^{-3}) and ρ^{FM} (5.24 g cm^{-3}) are the density of the PM and the FM components, respectively (Table 2). χ^{PM} and w^{FM} (and hence c^{FM}) were directly determined for $|H| \geq 20$ kOe from the average of the slopes of the straight lines fitted to both sides of the hysteresis curves (Fig. 7) and from the average of the values of magnetic moments m at the intercepts of the lines at $H = 0$, respectively (cf. the details shown for the Kevermes sample from 487.0 m in Fig. 7G). The χ^{PM} is of the order of magnitude of 10^{-6} emu g^{-1} Oe^{-1} (10^{-8} m^3 kg^{-1}) with a maximum variation within a factor of 2. The c_v^{FM} varies more than two orders of magnitude while the H_c (coercive field) is around 30–95 Oe with the exception of the Kevermes sample from 157.00 m (280 Oe) (Fig. 7E, Table 2).

The low fluctuation of the χ^{PM} revealed permits the investigation of the relationship between χ_{LF} and the magnetite concentration. The χ_{LF}, measured at 470 Hz, can be given as

$$\chi_{LF} = \left(1-c^{FM}\right)\chi^{PM} + c^{FM}\chi^{FM}, \qquad (3)$$

where χ^{FM} is the susceptibility of magnetite. Table 3 shows the calculated χ^{FM} together with the χ_{LF}, ρ_{av} and H_c where ρ_{av} is the average density of the sample, taking into account the concentration of the two components. χ^{FM} is of the order of magnitude of 10^{-2}–10^{-1} emu g^{-1} Oe^{-1} with a maximum variation within a factor of 2, except for two samples (Kevermes 123.50 m and 157.00 m).

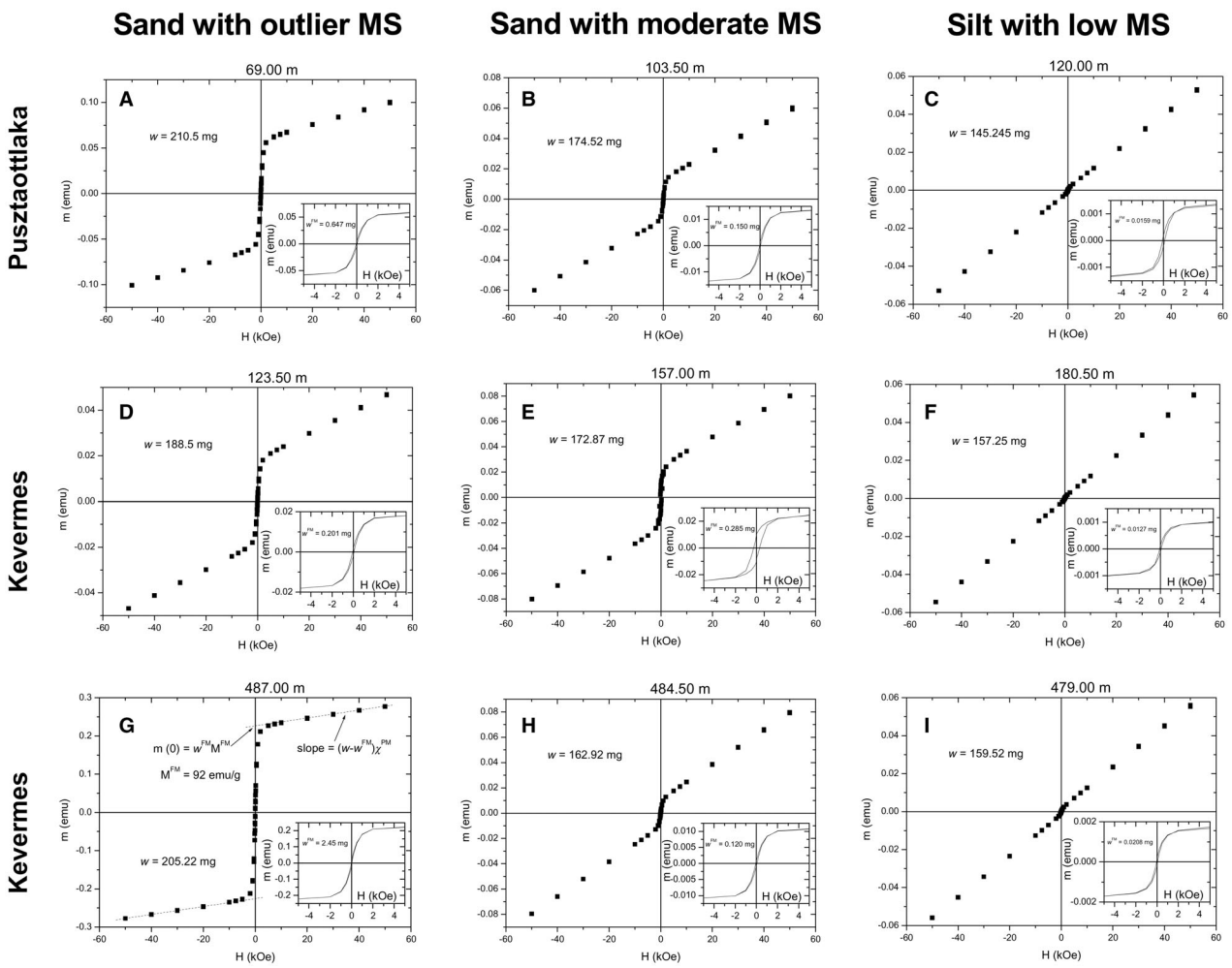

Fig. 7. Magnetic hysteresis curves (magnetic moment vs. magnetic field) for the sample set where w and w^{FM} are sample mass and mass of the FM (magnetite) component, respectively, $M^{FM} = 92$ emu g^{-1} is saturation magnetization of magnetite and χ^{PM} is mass susceptibility of the PM (sand) component. Insets: magnetic hysteresis of the ferrimagnetic magnetite contained in the sample after eliminating the PM contribution.

Since $\chi^{PM} \sim 10^{-6}$ emu g^{-1}Oe$^{-1} \ll \chi^{FM} \sim 10^{-2}$–$10^{-1}$ emu g^{-1} Oe^{-1}, expressing c^{FM} from Equation 3 we get

$$c^{FM} = \frac{\chi_{LF} - \chi^{PM}}{\chi^{FM} - \chi^{PM}} \cong \frac{1}{\chi^{FM}}\chi_{LF}. \quad (4)$$

Calculating with magnetite, c_v^{FM} and χ_{LF} present a reliable linear correlation ($R^2 = 0.982$; Fig. 8). Thus, based on the here presented hysteresis data, the variation of c^{FM} is reflected in, and can be estimated from the variation of χ_{LF} and the χ_{LF} peaks are driven by increases in c_v^{FM} superimposed on a relatively constant paramagnetic background.

As an exception, a depleted χ^{FM} can be seen in the Kevermes sample from 157.00 m, together with increased H_c (280 Oe) that indicates that the magnetite is magnetically much harder. Several factors have been reported as influencing the susceptibility and H_c of the magnetite like crystal anisotropy, stress, texture and domain structure (e.g. Day *et al.* 1977; Dunlop 1986; Kosterov 2002) even in Quaternary sediments (e.g. van Velzen & Dekkers 1999; Liu *et al.* 2003). In this case the SEM investigation of the related sample revealed the advanced chemical alteration of the magnetite (Fig. 6S measured points 26–28) and small (<0.5 µm) remnants of magnetite crystals (Fig. 6T measured points 29, 30). The reason for the increased value of χ^{FM} in the Kevermes 123.50 m sample being associated with an average H_c value is not yet known.

Time-series analyses

The susceptibility records were re-scaled for spectral investigations based on the correlated susceptibility peaks. The correlation target was the marine oxygen isotope stage (MIS) record based on the correlation of Dévaványa to MIS already proposed (Püspöki *et al.* 2021b: fig. 6). To compare the different facies

Table 3. Measured values of χ_{LF} (2nd column: volume susceptibility (SI); 4th column: mass susceptibility), ρ_{av} average density, χ^{FM} susceptibility of magnetite, H_c coercive field.

Sample	χ_{LF} (10^{-5}) (SI)	ρ_{av} (g cm^{-3})	χ_{LF} (10^{-5} emu g^{-1} Oe^{-1} or 10^{-8} kg m^{-3})	χ^{FM} (10^{-2} emu g^{-1} Oe^{-1})	H_c (Oe)
Pusztaottlaka 69.00 m	499.5	0.977	40.7/511	13.1	40
Pusztaottlaka 103.50 m	68.3	0.799	6.80/85.5	7.28	45
Pusztaottlaka 120.00 m	16.4	0.883	1.48/18.6	7	95
Kevermes 123.50 m	260	0.871	23.8/298	21.9	60
Kevermes 157.00 m	69	0.805	6.82/85.8	3.76	280
Kevermes 180.50 m	16	0.931	1.37/17.2	8.52	70
Kevermes 479.00 m	21	0.96	1.74/21.9	8.19	45
Kevermes 484.50 m	68	0.843	6.42/80.6	7.57	50
Kevermes 487.00 m	1541	0.887	138/1737	11.5	30

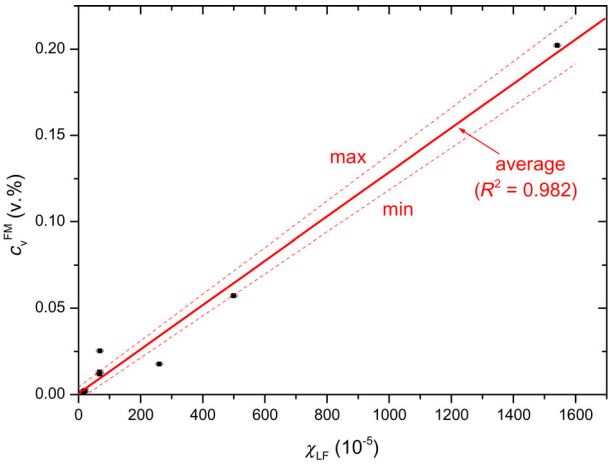

Fig. 8. Volume susceptibility of magnetite (c_v^{FM}) as a function of low-field magnetic susceptibility (χ_{LF}) for the nine selected samples. The points are the measured values, the solid line is a linear fit to the data, the dashed lines show the upper and lower limits of the values obtained from the error margins of the fit.

conditions, the MTM spectra of the Maros Fan obtained here are presented together with those from the reference Dévaványa and Jingbian sections (Ding *et al.* 2005; Fig. 9).

The most important feature of the Maros Fan spectra (Fig. 9B, C) is the statistically reliable (CL = 99%) occurrence of the ~41-ka cycles together with the occurrence of the customary ~100-ka cycles. Considering the source-proximal (Fig. 9B) to source-distal (Fig. 9C) position of the fluvial fan sections and the source-distal fluvial plain section (Fig. 9D), a decrease in the intensity of the ~41-ka cycles can be detected, while the occurrence of the ~100-ka cycles remains consistent. The most similar spectra in the group of terrestrial MS records are those of the Kevermes (Fig. 9B) and Jingbian (Fig. 9A) sections, where, beside the ~41- and ~100-ka cycles – the latter is shifted somewhat towards the higher (~82 ka) frequencies in both periodograms – a ~400-ka frequency of eccentricity can also be detected.

To ensure an independent check of the re-scaling and the possibility of joint investigation of different climate proxies, the gamma-ray logs of the Maros Fan sections, recording clay content proportional to grain-size variations, were also investigated spectrally (Fig. 9E, F). For these investigations the re-scaling was performed using the depth/time model derived from the magnetic susceptibility correlations. The results show that the same frequencies occur in the grainsize variations as in the MS records. In the Kevermes section (Fig. 9E) the ~41-ka cycle is statistically important (CL = 90%), while at Pusztaottlaka (Fig. 9F) the ~100-ka cycle is apparent.

This similarity of magnetic susceptibility and grain size-related gamma-ray plots may indicate that climate changes can affect both of these variables. At the same time the significant difference between the spectral intensities may be a result of the fact that the climate control operates in different ways. Moreover, in the case of grain-size variations, the spectrum is suppressed by other Quaternary event(s) – tectonic or overall fan development – that cause very high intensity at very low frequency causing the relatively low intensities of the fundamental Milankovitch frequencies.

Powers in magnetic susceptibility records, considered as significant with respect to a given confidence level in MTM spectra, are apparent at similar frequencies in the global wavelet spectra (Fig. 10). According to the scalograms, the Maros Fan sections show the ~41-ka cyclicity, predominantly between 1000 and 2500 ka especially in the V, VII and IX magnetic susceptibility cycles, while the ~84- and ~120-ka components of the ~100-ka eccentricity cycles can be detected throughout the Quaternary at the site. The extreme χ_{LF} value of the Kevermes section at MP10a suppresses significantly the relative scalogram values outside the dominance region of the extreme value (Fig. 10A). A truncation of this data set leaving out the lowermost part with the extreme value increases the significance of the ~84- and ~41-ka cycle frequencies to close to or even above the 95% confidence level, the latter in the V and IX magnetic susceptibility cycles (Fig. 10B).

Thus, the similarity of the Maros Fan sections to the globally relevant loess section is more than an accidental resemblance, it is also expressed in the spectral similarity of these records. However, a special feature of the Maros Fan sections is that both the ~41- and ~100-ka frequencies are more clearly expressed in the lower, >1000 ka part of the Quaternary record.

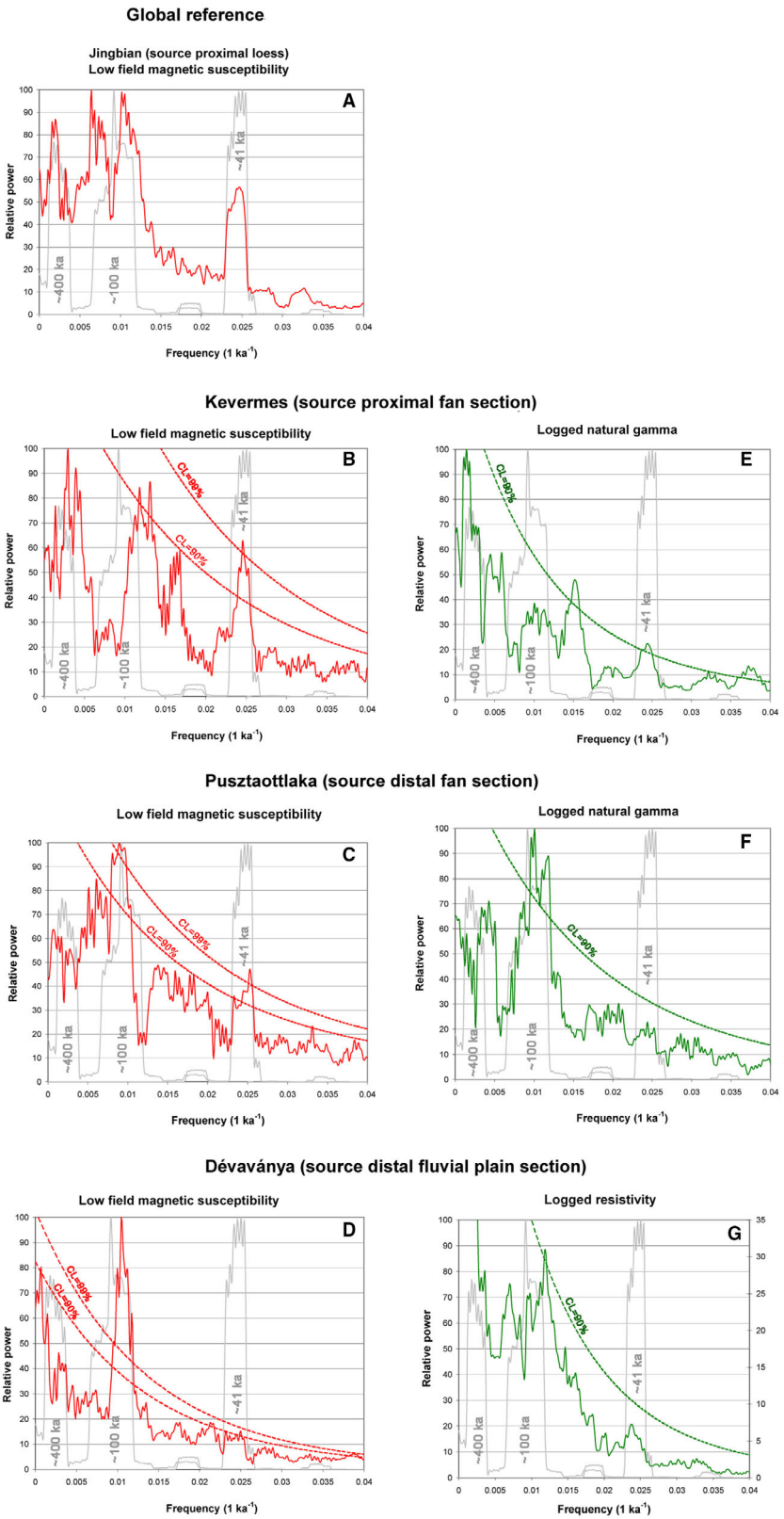

Fig. 9. MTM spectra of the complete reference boreholes of the Maros fluvial fan, Dévaványa borehole (Püspöki *et al.* 2021b) and Jingbian loess section (Ding *et al.* 2005).

Stratigraphy of the Maros Fan based on the correlation of measured and logged χ_{LF} records

Downhole logging of χ_{LF} in the Tótkomlós reference borehole and in more hydrogeological wells (e.g. Telekgerendás, Nagybánhegyes) was performed in the 1980s. In the log correlations presented here the reference boreholes and wells for which the logged χ_{LF} is available were also used. The χ_{LF} is plotted next to the gamma-ray, spontaneous potential and/or resistivity curves to allow comparison of the grain-size and susceptibility variations. One section is parallel with the sediment transport and contains the reference boreholes in the nearby Körös Basin (Fig. 11A), whilst the other is perpendicular to the axis of the Battonya Ridge and contains the Tótkomlós borehole, which allows a direct comparison of laboratory and logged χ_{LF} data (Fig. 11B).

The overall coarsening-upward nature of the sedimentary succession (cf. Weissmann *et al.* 2013), superimposed with the predominant occurrence of sandy channel facies on the upper part of the succession, was mentioned above. Now it can be seen that the lowest sand layer that is regionally coarser in the succession is attached to MP5 (~970 ka MIS 26), while the most apparent coarsening can be related to the 3a and MP3 MS maxima (~650, ~430 ka, i.e. within MIS 16 and 12) (Fig. 11A). This change in facies characteristics can be related to the changing hydrology related to the climatically triggered 'mid-Pleistocene transition' (MPT) (Gibbard & Lewin 2009) and to the onset of the extensive Middle Pleistocene glaciations, or rather their subsequent deglaciations, somewhat similar to that recorded by Šujan *et al.* (2018) corresponding to the onset of major Alpine glaciations.

Another important stratigraphical feature of the Maros Fan sections is the regular occurrence of stratigraphically relevant χ_{LF} maxima within well-correlated sandy layers. Thus, in the succession of the Maros Fan, stratigraphically relevant χ_{LF} maxima and regionally correlated sand bodies seem to be a related phenomenon, contrary to the Jászság Basin, for example (Püspöki *et al.* 2020), where χ_{LF} maxima can occur both in sandy channel and fine overbank facies deposits alike.

In Fig. 11A the logged susceptibility at Telekgerendás strongly records the magnetic susceptibility cycles, indicating that the Quaternary base was not reached here. An important phenomenon also recorded by the logged χ_{LF} at Telekgerendás is the disappearance of MP7 towards the source-distal settings. In Fig. 11B the Regional Unconformity-1 (Fig. 5) is confirmed by a logged susceptibility at Nagybánhegyes, which represents a transitional position between the basin centre and the top of the Battonya Ridge. This regional unconformity demonstrates the Pleistocene structural activity of the Battonya Ridge.

Discussion

The mountain permafrost origin of the χ_{LF} signal in the Maros fluvial fan deposits

The climate-related variation of χ_{LF} in fluvial deposits has been repeatedly found in the Pannonian Basin Quaternary fluvial succession. However, the interpretation of the phenomenon has remained incomplete.

First interpretations considered the variation of the χ_{LF} simply as the result of the detrital origin of ferri- and paramagnetic minerals based on the seeming coincidence of grain size and χ_{LF} (e.g. Nádor *et al.* 2003). This interpretation was questioned subsequently based on two phenomena: (i) outlying χ_{LF} maxima were revealed also in silty overbank deposits (Püspöki *et al.* 2020), (ii) outlying χ_{LF} maxima occurred only in the Quaternary part of the fluvial succession, enabling at the same time the indication of the Quaternary base (Püspöki *et al.* 2020, 2021b).

Thus, as an alternative explanation, the early post-glacial mountain permafrost-related interpretation of the χ_{LF} maxima in the Quaternary sequence was proposed (Püspöki *et al.* 2016, 2020, 2021a). This was confirmed by the regular coincidence of the regional occurrence of mountain permafrost-related fluvial χ_{LF} maxima and extreme increases of the global ice volume (Püspöki *et al.* 2021b).

In the case of the Maros Fan this interpretation of the χ_{LF} is also relevant. Considering the Tótkomlós section (Fig. 11B), the outlying χ_{LF} maxima are apparently confined to the Quaternary part of the fluvial succession. At the same time, based on cross plots with the recorded grain-size proxies i.e. the logged resistivity and gamma-ray (Fig. S3A, B, E), there is no correlation between grain-size related parameters and χ_{LF} (Fig. S3G, H).

The data from the Maros Fan presented here yield two more arguments to support the permafrost-related explanation of the fluvial χ_{LF} variations. Firstly, the hysteresis investigations revealed that the χ_{LF} is directly related ($R^2 = 0.98$) to the fresh magnetite content of the sediments only (Fig. 8). The paramagnetic fraction and even the weathered, multiply reworked magnetite content of the Quaternary sands, detected, e.g. in the Kevermes sample from 157-m depth (Fig. 6S, T), have no significant effect on susceptibility variations. Secondly, the absolute values of χ_{LF} gradually decrease from the source-proximal Maros Fan, towards the source-distal settings represented by the Dévaványa, Szarvas and Mindszent sections (Fig. 4). This indicates that the detected fresh magnetite content of the fluvial load is transported from the surrounding upland catchment region towards the basin centre, which confirms the origin and explanation of the fluvial χ_{LF} values.

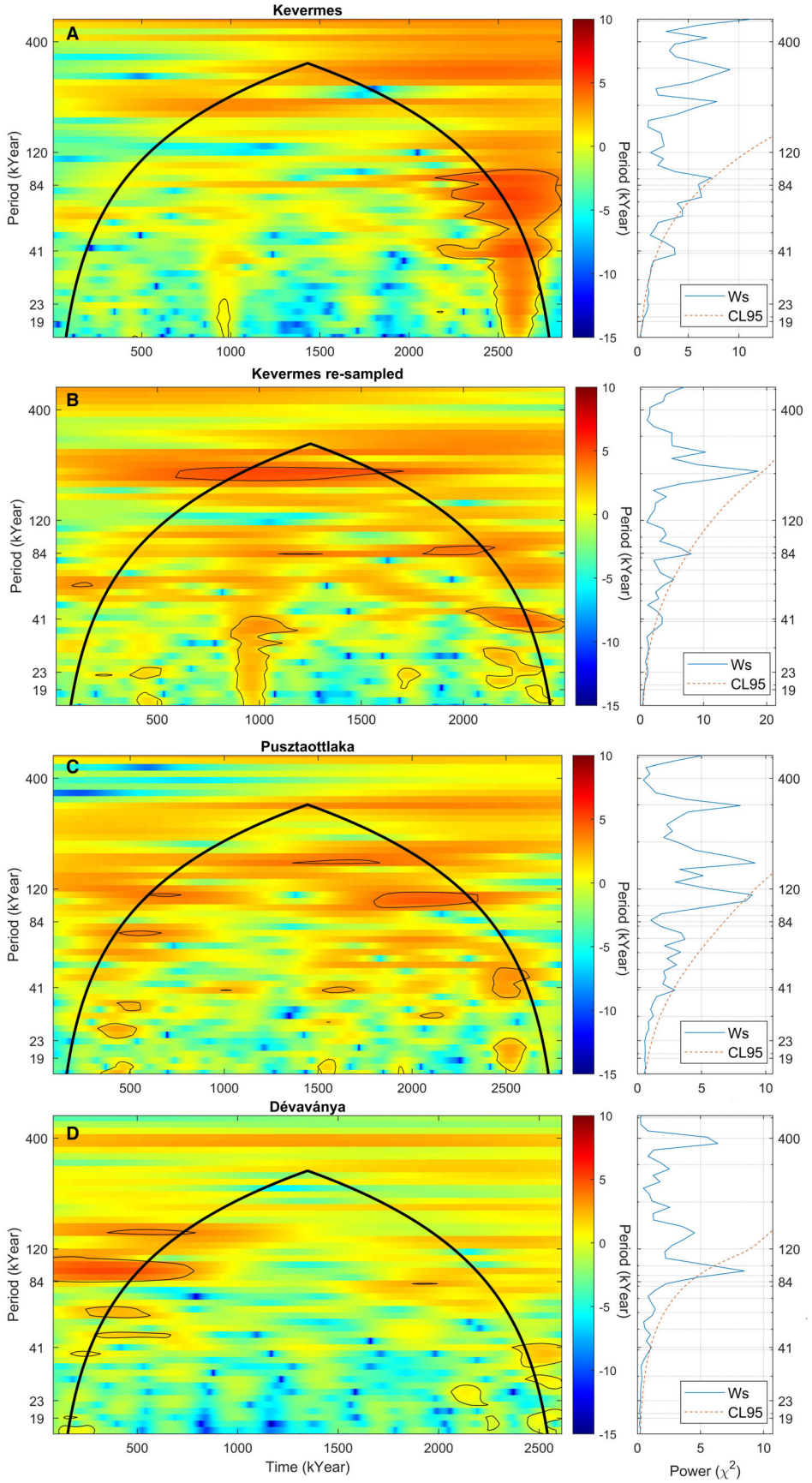

Fig. 10. Wavelet scalograms of the susceptibility signals of the Maros Fan and reference sections obtained with continuous wavelet transformation making use of the Morlet mother wavelet. The colour scale represents the logarithms of the wavelet powers. The thick black curve represents the cone of influence of the transform, while the thin black curves enclose those areas where the wavelet power exceeds the 95% confidence level of a red-noise process (Torrence & Compo 1998). To right the global wavelet spectra of the susceptibility records, with the 95% confidence level of a red-noise background.

Joint sedimentary and χ_{LF} cycles of the fluvial fan deposits

Fluvial fans were evoked in the Introduction as depositional landforms controlled by climate changes through variations in hydraulic properties of the distributive avulsive drainage and in physical processes of the catchment. This should be considered when interpreting the regionally extended sand strata containing the stratigraphically relevant χ_{LF} maxima in the Maros Fan.

Weissmann *et al.* (2002) showed that the climate control on hydraulic properties can cause peculiar stratigraphical architecture of fluvial fans. During 'glacial recession' the 'intersection point' of a fluvial fan, i.e. the boundary of source-proximal erosion and source-distal accumulation, is shifted to a source-proximal position. This proximal location of the intersection point promotes the deposition of channel sand across the entire fan. This 'glacial recession' was interpreted as the 'High Accumulation Space' period analogous to the marine highstand deposits. It is characterized by high-frequency autocyclic lobe switching and low-level pedogenetic alteration of open-fan deposits. It was also raised by Weissmann *et al.* (2002), that this 'glacial recession' may be contemporaneous with the sediment release from glaciers during deglaciation (e.g. Clark 1987; Church & Slaymaker 1989).

Based on the glacial setting of the Carpathians in the Pleistocene (Popescu *et al.* 2017), these glacially driven sedimentary cycles can be assumed to be represented in the Quaternary fluvial succession of the Maros Fan. Moreover, the intimate relation between regionally correlated sand strata and 'early postglacial' permafrost-related χ_{LF} maxima confirms the supposition that the 'glacial recession' periods (i.e. climatic amelioration) are contemporaneous with the sediment release from glaciers during deglaciation. The temporal coincidence of the regionally correlated sand units of 'glacial recession' and 'early postglacial' χ_{LF} maxima, occurring only in the Quaternary part of the fluvial fan succession, can be interpreted as the direct consequence of the Quaternary climate changes affecting both the hydraulic properties and catchment-area permafrost conditions.

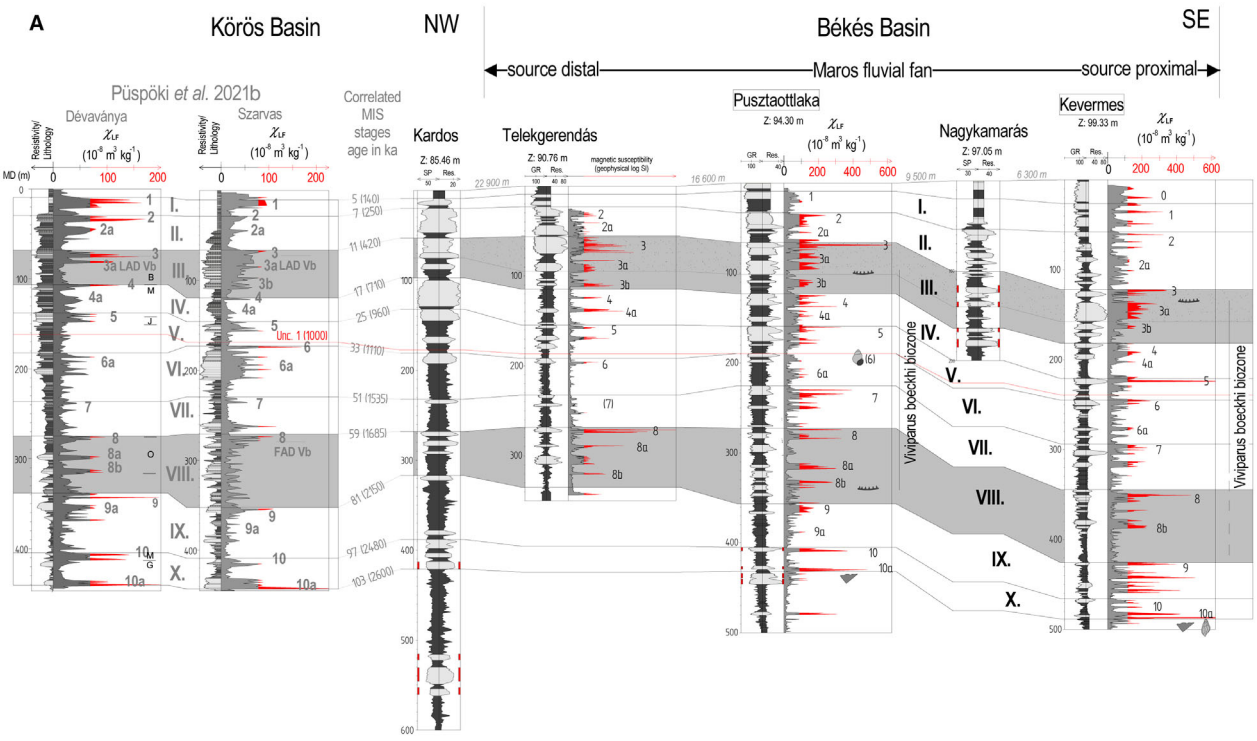

Fig. 11. Log correlation sections of the Maros fluvial fan, supported by measured and logged low-field magnetic susceptibility records. For the position of the sections see Fig. 2. A. Dip oriented section presenting the contact of the Békés and Körös Basins. B. Strike oriented section presenting the contact of the Békés Basin and the Battonya Ridge. The upper quartile (Q3) range together with the outlier and extreme values are highlighted by red colour in χ_{LF} tracks.

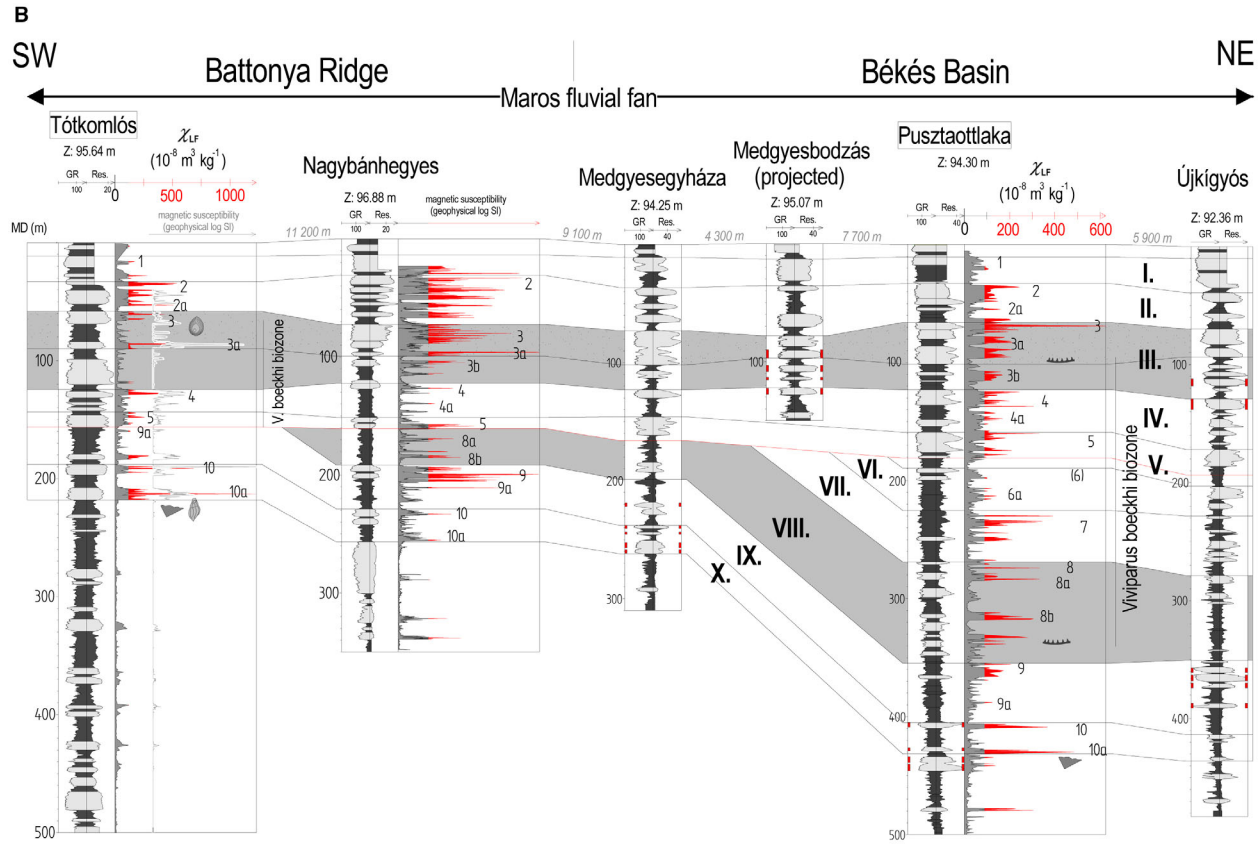

Fig. 11. (Continued)

In the case of the Maros Fan the duration of the increased avulsion dynamics in 'glacial recession' and contemporaneous 'early postglacial' χ_{LF} episodes can be determined. Based on the weather-sensitive nature of magnetic minerals, the 'early postglacial' magnetic susceptibility episodes have been interpreted as short-term events representing a few thousand years (Püspöki *et al.* 2016). At the same time, based on the published OSL determinations (Kiss *et al.* 2014), the high-frequency autocyclic avulsions enabled the accumulation of channel sand deposits over the entire surface of the Maros Fan within a maximum 10-ka time interval (Fig. 1C). Thus, the overall accumulations of sandy open-fan deposits of increased magnetite content in the 'glacial recession' periods represent relatively rapid short-term events within the Milankovitch-scale cycles.

The reason for and importance of the obliquity driven χ_{LF} cycles in fluvial fan records

The occurrence of ~41 ka cycles in the fluvial fan deposits is a new observation. Thus far, it has been assumed that the fluvial conditions, characterized by frequent unconformities or hiatuses, were favourable only for the preservation of ~100-ka cycles of magnetic susceptibility. Nevertheless, the occurrence of the ~41-ka cycles in the Maros Fan succession cannot be interpreted as a result of a high sedimentation rate. The sedimentation rate in the Körös Basin and the Makó Trough is similar or even greater than that of the Maros Fan. However, the ~41-ka cycles cannot be detected in these source-distal fluvial settings (Püspöki *et al.* 2021a, b).

It is the anomalously high value of magnetic susceptibility in the source-proximal settings (Fig. 4), and the special stratigraphical architecture of the fluvial fan discussed above, that is most likely to be responsible for the occurrence of the high-frequency susceptibility variations. The climate-controlled rearrangements of the avulsive distributive hydraulic conditions, in concert with the climate-controlled variations in the permafrost-related magnetic fraction derived from the catchment, could amplify the otherwise strong magnetic susceptibility signal in the source-proximal fluvial succession. The higher intensity of ~41-ka cycles in the source-proximal Kevermes section may indicate that the avulsion frequency is higher in the proximal narrower end of the fan, enabling a better preservation of the high-frequency changes.

Having been a local phenomenon, this could be simply a particular condition, which could be interesting as a unique section recording the high-frequency variations in permafrost development in the Carpathians. However, it has to be considered that fluvial and – from this aspect

most presumably similar – alluvial fans are widespread recent depositional landforms of the Eurasian mountain range and were surely also an equally significant occurrence during the repeated Quaternary deglaciations. This was so, regardless of whether the tectonic conditions enabled the preservation of the long-term sedimentary record or not. Thus, obliquity-driven grain-size and associated magnetic susceptibility variations in source-proximal distributive fluvial systems can reasonably be assumed in this extensive geographical region.

Fluvial–aeolian cross-facies correlations – perspectives and problems

The similarity of the χ_{LF} records measured in the Maros fluvial fan to those of the Jingbian section (Figs 5, 9) suggests the possibility of cross-facies correlations. As a section of the Chinese Loess Plateau (CLP) plotted in the stratigraphical chart of the International Commission on Stratigraphy (Cohen & Gibbard 2019), the Jingbian section would usually be considered to follow the classic CLP magnetic soil enhancement model; however, as a section situated close to the desert margin, the Jingbian section has two special features.

The first is that the precise luminescence-based chronology of the past 250 ka (Stevens *et al.* 2018) revealed that although the palaeosol units coincide with the interglacial phases in the Jingbian section, the loess units are associated with stadials within interglacials, instead of glacials. Glacial phases are represented by ~50-ka hiatuses interpreted to be the result of aeolian denudation due to the increased intensity of the winter monsoon, potentially challenging somewhat the justification of the Jingbian section as an ideal global reference. Thus, the Jingbian section is very similar to the fluvial fan sections presented here, considering that both facies are dominated by interglacial sedimentation and the glacial phases are underrepresented.

The second important feature is that the Jingbian section records a conflict between χ_{LF} and grain-size variations pointed out by Ding *et al.* (2005). The sand-sized particle record at Jingbian indicates significant expansion of the desert in northern China at ~2.6, ~1.2, ~0.7 and ~0.2 Ma and thus a southward retreat of the monsoon rainfall belt. This contradicts the χ_{LF} record of the same section, which records a significant increase in susceptibility values usually interpreted as a summer-monsoon proxy. Thus, it was suggested that the long-term increase in susceptibility values in loess sediments from the Early to Late Pleistocene is significantly influenced by factors other than the summer monsoon, among which the effect of dust sources may be very important. Other studies also revealed that in several CLP sections, the principal carrier of magnetization is of detrital origin (e.g. Sun & Liu 2000). Thus, the possible impacts of dust sources were raised; however, they were mostly explained by climate-forced changes in wind direction or intensity, or by any significant change in the catchment topography.

Based on the records presented here it could also be considered that the fluvial (and alluvial) fans, as potential sources of loess material, have their own unique combination of facies and magnetic characteristics. During the 'glacial recession' periods the increased rate of avulsion favours enhanced wind erosion and air transportation of particles, while the increased proportion of magnetite in the 'early postglacials' causes increased χ_{LF} of this air-transported dust. Based on the χ_{LF} data, this increase in the fresh magnetite content of the fluvial load is of several orders of magnitude. This climate-controlled spreading of permafrost-related magnetite in fan deposits and related dusts occurs during deglaciations, i.e. just before the 'interglacial' palaeosol formation in loess sections.

Of course, this explanation can only be confirmed based on extended investigations of the Asian Quaternary fluvial fan records. Nevertheless, assuming a similarity of mountain permafrost and winter monsoon proxies in Asian continental regions would be a reasonable basis for comparison of the evidence. Moreover, this could also explain the similarity of the long-term European and Asian χ_{LF} records in the context of the mountain permafrost development of the mid-latitude upland region in the periglacial zone, thus providing new perspectives for continental scale terrestrial correlations and comparisons of terrestrial and marine proxy records (cf. Püspöki *et al.* 2021a).

As a consequence of the significantly varying accumulation rates and frequent hiatuses, together with the limited resolution of age control, these fluvial–loess correlations can be performed only at the first order level, i.e. MI Stage units, similar to the continental scale correlation of the loess sections (reviewed by Marković *et al.* 2018) and can be discussed in the context of the 'siltworm route' model (Smalley *et al.* 2009). Thus, in these correlations the climate-phase of the different facies units is critical when attempting to confirm the correlation and explain the underlying physical phenomenon.

From this perspective it is important to note that the χ_{LF} maxima in the fluvial Quaternary of the Pannonian Basin can be considered an early postglacial phenomenon, based on the results of the joint investigation of χ_{LF} and clay mineral properties in the Dévaványa section (Püspöki *et al.* 2016: figs 10, 11), while the soils representing the warm periods in the fluvial sections have low χ_{LF} values (Püspöki *et al.* 2016, 2020). At the same time the χ_{LF} maxima in the Jingbian section are clearly related to the interglacial accretionary soils (e.g. Ding *et al.* 1995), the age of the latter also confirmed by precise luminescence dating (Stevens *et al.* 2018). This apparent phase difference can be interpreted to be a result of the geographical difference. The fluvial upland catchments surrounding the Pannonian Basin were strongly affected by Atlantic Westerlies during the

interglacials, while those of the Asian continental desert regions were situated west of the summer monsoon rainfall belt. The intensification of the Westerlies in the interglacial events (e.g. Obreht *et al.* 2017) enhanced the disappearance of the fresh magnetic minerals from the fluvial loads in Europe, while in the Asian continental regions the 'postglacial fluvial magnetic episodes' could extend into the later phase of the interglacial periods as a result of the lower intensity of weathering.

These cross-facies correlation possibilities can potentially reinforce the challenged stratigraphical importance of the source-proximal Jingbian section, however, it can be considered rather as a reference site for long-term cross-facies correlations between Quaternary fluvial and aeolian systems than as a continuous aeolian record. It is also important to note that while in the Jingbian CLP section the χ_{LF} maxima coincide closely with palaeosols, in several loess sections in Siberia, Alaska and NW China (e.g. Ily Basin) the χ_{LF} maxima do not overlap with palaeosols but occur in loess, and the material is not, or is only sub-dominantly superparamagnetic (e.g. Begét *et al.* 1990; Chlachula *et al.* 1998; Chen *et al.* 2012). In these cases, the χ_{LF} peaks were also attributed to climatic changes in wind strength (Begét *et al.* 1990; Chlachula *et al.* 1998; Evans & Heller 2001) and to possible effects of local source materials (e.g. Chen *et al.* 2012). However, the climate-forced magnetic susceptibility cycles of the fluvial source regions can also be considered in these cases as a possible influence on the χ_{LF} peaks.

Conclusions

- The Quaternary Maros fluvial fan deposits record apparent ~41-ka cycle ~100-ka cycles, and the stratigraphical appearance together with the spectral characteristics strongly resemble those of globally relevant loess sections.
- Based on frequency dependent low-field susceptibility and hysteresis investigations, the fluvial fan susceptibility is non-superparamagnetic, and according to the SEM-EDAX investigations it can be attributed to the fresh detrital magnetite grains of various grain sizes (50–150 and 2–20 μm) originating from the catchment area as a result of 'early postglacial' permafrost degradation.
- Hysteresis investigations demonstrated that neither the paramagnetic fraction nor the weathered and/or reworked magnetite grains can influence the magnetic susceptibility records. Instead, the low-field magnetic susceptibility values show a strong linear correlation ($R^2 = 0.98$) with the fresh detrital magnetite fraction.
- Comparison of laboratory and field susceptibility measurements demonstrated that wireline logging of magnetic susceptibility can effectively help data acquisition in hydrogeological surveys of Quaternary terrestrial reservoirs.
- The correspondence of regionally correlated sand strata and the 'early postglacial' 'magnetic susceptibility events' confirms the already established sequence stratigraphical model, which interpreted the high frequency autocyclic lobe switching of sand-dominated open-fan deposits as 'High Accumulation Space' related to 'glacial recession'.
- The good preservation of ~41-ka cycles in fluvial fan deposits can be attributed to the high value of magnetic susceptibility of fluvial loads deposited in the source-proximal settings and to the specific stratigraphical architecture of the distributive depositional landforms.
- The 'early postglacial' spreading of permafrost-related magnetite grains on the surface of fluvial fans just in the 'glacial recession' periods, that is also characterized by increased frequency of autocyclic lobe switching in open-fan deposits, is a relevant phenomenon that should be considered when looking for possible source material of aeolian deposits.

Acknowledgements. – We express special thanks to the Paleomagnetic Laboratory staff under the leadership of Prof. Emő Márton for their generous help ensuring safe and professional conditions for the time-consuming measurements during the heavy pandemic times and Prof. Csaba Cserháti and Laura Juhász for their willing help in performing the SEM investigations. We also thank the reviewers, O. Mandic and the anonymous reviewer, for their constructive suggestions on how to improve the original manuscript. During the research work ZP was a member of MTA-ME Geoengineering Research Group, Hungary 3515 Miskolc-Egyetemváros. The Wigner Research Centre for Physics utilizes the research infrastructure of the Hungarian Academy of Sciences and is operated by the Eötvös Loránd Research Network (ELKH) Secretariat (Hungary).

Author contributions. – ZP planned the research, led the sampling and laboratory measurements and wrote the paper with input from all authors. PLG discussed the context of the investigations and co-wrote the paper. LFK undertook the hysteresis investigations and wrote the related section. RWM took part in sampling and co-wrote the paper. ET-B conducted the magnetic separations and discussed the interpretation of SEM-EDAX data. ZK carried out the SEM investigations and discussed the related section. BS documented the fossils and discussed the related section. VM performed the SRTM data management and geomorphological analysis. PK performed the wavelet investigations. DK took part in sampling and discussion of the correlations. FS took part in sampling and time-series analyses. FV took part in database development and discussing the text. KD took part in database development and discussion of correlations. LB performed the seismic investigations. TS took part in log correlations and discussing the text. ÁR-S took part in database development and discussing the text. TF managed the project, took part in time-series interpretations and discussed the text.

Data availability statement. – The data that support the findings of this study are available from the corresponding author upon reasonable request.

References

Begét, J. E., Stone, D. B. & Hawkins, D. B. 1990: Paleoclimatic forcing of magnetic susceptibility variations in Alaskan loess during the late Quaternary. *Geology 18*, 40–43.

Blair, T. C. & McPherson, J. G. 1994: Alluvial fans and their natural distinction from rivers based on morphology, hydraulic processes, sedimentary processes and facies. *Journal of Sedimentary Research A64*, 451–490.

Bull, W. B. 1977: The alluvial fan environment. *Progress in Physical Geography 1*, 222–270.

Chen, Q., Liu, X. M., Heller, F., Hirt, A. M., Lü, B., Guo, X. L., Mao, X. G., Chen, J. S., Zhao, G. Y., Feng, H. & Guo, H. 2012: Susceptibility variations of multiple origins of loess from the Ily Basin (NW China). *Chinese Science Bulletin 57*, 1844–1855.

Chlachula, J., Evans, M. E. & Rutter, N. W. 1998: A magnetic investigation of a late Quaternary loess/palaeosol record in Siberia. *Geophysical Journal International 132*, 128–132.

Church, M. & Ryder, J. M. 1972: Paraglacial sedimentation: a consideration of fluvial processes conditioned by glaciation. *Geological Society of America Bulletin 83*, 3059–3072.

Church, M. & Slaymaker, O. 1989: Disequilibrium of Holocene sediment yield in glaciated British Columbia. *Nature 337*, 452–454.

Clark, M. J. 1987: The alpine sediment system: a context for glacio-fluvial processes. *In* Gurnell, A. M. & Clark, M. J. (eds.): *Glacio-Fluvial Sediment Transfer: An Alpine Perspective*, 9–31. John Wiley & Sons, Chichester.

Cohen, K. M. & Gibbard, P. L. 2019: Global chronostratigraphical correlation table for the last 2.7 million years, version 2019 QI-500. *Quaternary International 500*, 20–31.

Cooke, H. B. S., Hall, J. M. & Rónai, A. 1979: Paleomagnetic, sedimentary and climatic records from boreholes at Dévaványa and Vésztő, Hungary. *Acta Geologica Hungarica 22*, 89–109.

Csato, I., Tóth, S., Catuneau, O. & Granjeon, D. 2015: A sequence stratigraphic model for the Upper Miocene–Pliocene basin fill of the Pannonian Basin, eastern Hungary. *Marine and Petroleum Geology 66*, 117–134.

Cullity, B. D. & Graham, C. D. 2009: *Introduction to Magnetic Materials*. 183 pp. John Wiley and Sons, Hoboken.

Day, R., Fuller, M. & Schmidt, V. A. 1977: Hysteresis properties of titanomagnetites: grain-size and compositional dependence. *Physics of the Earth and Planetary Interiors 13*, 260–267.

Dearing, J. A., Dann, R. J. L., Hay, K., Lees, J. A., Loveland, P. J., Maher, B. A. & O'Grady, K. 1996: Frequency-dependent susceptibility measurements of environmental materials. *Geophysical Journal International 104*, 228–240.

Deng, C., Zhu, R., Verosub, K. L., Singer, M. J. & Vidic, N. J. 2004: Mineral magnetic properties of loess/paleosol couplets of the central loess plateau of China over the last 1.2 Myr. *Journal of Geophysical Research 109*, B01103, https://doi.org/10.1029/2003JB002532.

Ding, Z. L., Derbyshire, E., Yang, S. L., Sun, J. M. & Liu, T. S. 2005: Stepwise expansion of desert environment across northern China in the past 3.5 Ma and implication for monsoon evolution. *Earth and Planetary Science Letters 237*, 45–55.

Ding, Z., Liu, T., Rutter, N. W., Yu, Z., Guo, Z. & Zhu, R. 1995: Ice-volume forcing of east Asian winter monsoon variations in the past 800,000 years. *Quaternary Research 44*, 149–159.

Dormann, J. L., Fiorani, D. & Tronc, E. 1997: Magnetic relaxation in fine-particle systems. *In* Prigogine, I. & Rice, S. (eds.): *Advances in Chemical Physics*, 343–364. Wiley, New York.

Dunlop, D. J. 1986: Hysteresis properties of magnetite and their dependence on particle size: a test of pseudo-single-domain remanence models. *Journal of Geophysical Research 91*, 9569–9584.

Dunlop, D. J. & Özdemir, Ö. 1997: *Rock Magnetism: Fundamentals and Frontiers*. 573 pp. Cambridge University Press, New York.

Evans, M. E. & Heller, F. 2001: Magnetism of loess/palaeosol sequences: recent developments. *Earth-Science Reviews 54*, 129–144.

Foufoula-Georgiou, E. & Kumar, P. (eds.) 1994: *Wavelets in Geophysics*. 384 pp. Academic Press, San Diego.

Franyó, F. 1992: Geological and hydrogeological conditions explored by borehole Tótkomlós III/P in SE Hungary. *A Magyar Állami Földtani Intézet Jelentése az 1990. évről*, 211–228.

Frostrick, L. E., Linsey, T. K. & Reid, I. 1992: Tectonic and climatic control of Triassic sedimentation in the Beryl Basin, northern North Sea. *Journal of the Geological Society 149*, 13–26.

Gibbard, P. L. & Lewin, J. 2009: River incision and terrace formation in the late Cenozoic of Europe. *Tectonophysics 474*, 41–55.

Grow, J. A., Mattick, R. E., Bérczi-Makk, A., Péró, C., Hajdú, D., Pogácsás, G., Várnai, P. & Varga, E. 1994: Structure of the Békés Basin inferred from seismic reflection, well and gravity data. *In* Teleki, P. G., Mattick, R. E. & Kókai, J. (eds.): *Basin Analysis in Petroleum Exploration*, 1–38. Kluwer Academic Publishers, Dordrecht.

Haas, J., Budai, T., Csontos, L., Fodor, L., Konrád, G. & Koroknai, B. 2014: *Geology to the Pre-Cenozoic basement of Hungary. Explanatory notes of the "Pre-Cenozoic geological map of Hungary" (1: 500000)*. 73 pp. Geological and Geophysical Institute of Hungary, Budapest.

Halaváts, G. 1888: A szentesi artézi kút. *Magyar Királyi Földtani Intézet Évkönyve 8*, 157–186.

Hartley, A. J., Weissman, G. S., Nichols, G. J. & Warwick, G. L. 2010: Large distributive fluvial systems: characteristics, distribution and controls on development. *Journal of Sedimentary Research 80*, 167–183.

Harvey, A. M. 2012: The coupling status of alluvial fans and debris cones: a review and synthesis. *Earth Surface Processes and Landforms 37*, 64–76.

Harvey, A. M., Stokes, M., Mather, A. & Whitfield (née Mather), E. 2016: Spatial characteristics of the Pliocene to modern alluvial fan successions in the uplifted basins of Almeria: S.E. Spain: review and regional synthesis. *In* Ventra, D. & Clarke, L. E. (eds.): *Geology, Geomorphology of Alluvial and Fluvial Fans: Terrestrial, Planetary Perspectives*, 65–78 *Geological Society, London, Special Publication 440*.

Heider, F., Bock, J. M., Hendy, I., Kennett, J. P., Matzka, J. & Schneider, J. 2001: Latest Quaternary rock magnetic record of climatic and oceanic change, Tanner Basin, California borderland. *Geological Society of America Bulletin 113*, 346–359.

Kiss, T., Sümeghy, B. & Sipos, G. 2014: Late Quaternary paleodrainage reconstruction of the Maros River alluvial fan. *Geomorphology 204*, 49–60.

Knobel, M., Nunes, W. C., Socolovsky, L. M., De Biasi, E., Vargas, J. M. & Denardin, J. C. 2008: Superparamagnetism and other magnetic features in granular materials: a review on ideal and real systems. *Journal of Nanoscience and Nanotechnology 8*, 2836–2857.

Koroknai, B., Wórum, G., Tóth, T., Koroknai, Z., Fekete-Németh, V. & Kovács, G. 2020: Geological deformations in the Pannonian Basin during the neotectonic phase: new insights from the latest regional mapping in Hungary. *Earth-Science Reviews 211*, 1–30.

Kosterov, A. 2001: Magnetic hysteresis of pseudo-single-domain and multidomain magnetite below the Verwey transition. *Earth and Planetary Science Letters 186*, 245–253.

Kosterov, A. 2002: Low-temperature magnetic hysteresis properties of partially oxidized magnetite. *Geophysical Journal International 149*, 796–804.

Kosterov, A. 2003: Low-temperature magnetization and AC susceptibility of magnetite: effect of thermomagnetic history. *Geophysical Journal International 154*, 58–71.

Kretzoi, M. & Kroloppp, E. 1972: Oberpliozäne und quartäre Stratigraphie des Alföld (Grosse Ungarischen Tiefebene) aufgrund paläontologischer Angaben. *Földrajzi Értesítő 21*, 133–158 (in Hungarian with German abstract).

Krolopp, E. 1976: Felkérés a malakológus kollégákhoz. *Soosiana 4*, p. 4.

Krolopp, E. 1982: *Malacological investigation of Tótkomlós borehole*. 8 pp. Hungarian Geological, Geophysical and Mining Datastore, Budapest (in Hungarian).

Krolopp, E. 1983a: *Malacological investigation of Pusztaottlaka borehole*. 6 pp. Hungarian Geological, Geophysical and Mining Datastore, Budapest (in Hungarian).

Krolopp, E. 1983b: *Malacological investigation of Kevermes borehole*. 5 pp. Hungarian Geological, Geophysical and Mining Datastore, Budapest (in Hungarian).

Krolopp, E. 1995: Biostratigraphic division of Pleistocene formations in Hungary, according to their mollusc fauna. *In* Füköh, L. (ed.): *Quaternary Malacostratigraphy in Hungary*, 17–78. *Malacological Newsletter, Supplement 1*.

Krolopp, E. 2002: Taxonomic, faunistic, stratigraphic and paleoecological evaluation of the Hungarian Pleistocene mollusc fauna. *Malacological Newsletter 31*, 4–57.

Laskar, J., Robutel, P., Joutel, F., Gastineau, M., Correia, A. C. M. & Levrard, B. 2004: A long-term numerical solution for the insolation quantities of the Earth. *Astronomy and Astrophysics 428*, 261–285.

Leonhardt, R. 2006: Analyzing rock magnetic measurements: the Rock-MagAnalyzer 1.0 software. *Computers & Geosciences 32*, 1420–1431.

Liu, Q., Banerjee, S. K., Jackson, M. J., Chen, F., Pan, Y. & Zhu, R. 2003: An integrated study of the grain-size-dependent magnetic mineralogy of the Chinese loess/paleosol and its environmental significance. *Journal of Geophysical Research 108*, 2437, https://doi.org/10.1029/2002JB002264.

Marković, S. B., Stevens, T., Mason, J., Vandenberghe, J., Yang, S., Veres, D., Újvári, G., Timar-Gabor, A., Zeeden, C., Guo, Z., Hao, Q., Obreht, I., Hambach, U., Wu, H., Gavrilov, M. B., Rolf, C., Tomic, N. & Lehmkuhl, F. 2018: Loess correlations – between myth and reality. *Palaeogeography, Palaeoclimatology, Palaeoecology 509*, 4–23.

Mattick, R. E., Rumpler, J., Ujfalusy, A., Szanyi, B. & Nagy, I. 1994: Sequence stratigraphy of the Békés basin. *In* Teleki, P. G., Mattick, R. E. & Kókai, J. (eds.): *Basin Analysis in Petroleum Exploration*, 39–66. Kluwer Academic Publishers, Dordrecht.

Moscariello, A. M. 2018: Alluvial fans and fluvial fans at the margins of continental sedimentary basins: geomorphic and sedimentological distinction for geo-energy exploration and development. *In* Ventra, D. & Clarke, L. E. (eds.): *Geology, Geomorphology of Alluvial and Fluvial Fans: Terrestrial, Planetary Perspectives*, 215–244 *Geological Society, London, Special Publication 440*.

Muxworthy, A. R. & McClelland, E. 2008: Review of the low-temperature magnetic properties of magnetite from a rock magnetic perspective. *Geophysical Journal International 140*, 101–114.

Nádor, A., Lantos, M., Tóth-Makk, Á. & Thamó-Bozsó, E. 2003: Milankovitch-scale multy-proxy records from fluvial sediments of the last 2.6 Ma, Pannonian Basin, Hungary. *Quaternary Science Reviews 22*, 2157–2175.

Nicholls, G. 2017: High resolution estimates of rates of depositional processes from an alluvial fan succession in the Miocene of the Ebro Basin, northern Spain. *In* Ventra, D. & Clarke, L. E. (eds.): *Geology, Geomorphology of Alluvial and Fluvial Fans: Terrestrial, Planetary Perspectives*, 159–174 *Geological Society, London, Special Publications 440*.

Obreht, I., Hambach, U., Veres, D., Zeeden, C., Bösken, J., Stevens, T., Markovic, S. B., Klasen, N., Brill, D., Burow, C. & Lehmkuhl, F. 2017: Shift of large-scale atmospheric systems over Europe during late MIS 3 and implications for Modern Human dispersal. *Nature Scientific Reports 7*, 5848, https://doi.org/10.1038/s41598-017-06285-x.

Özdemir, Ö. & Dunlop, D. J. 2010: Hallmarks of maghemitization in low temperature remanence cycling of partially oxidized magnetite nanoparticles. *Journal of Geophysical Research 115*, B02101, https://doi.org/10.1029/2009JB006756.

Paillard, D. L., Labeyrie, M. A. & Yiou, P. 1996: Macintosh program performs time-series analysis. *Eos, Transactions of the American Geophysical Union 77*, p. 379.

Paterson, G. A., Zhao, X., Jackson, M. & Heslop, D. 2018: Measuring, processing, and analyzing hysteresis data. *Geochemistry, Geophysics, Geosystems 19*, 1925–1945.

Popescu, R., Onaca, A., Urdea, P. & Vespremeanu-Stroe, A. 2017: Spatial distribution and main characteristics of alpine permafrost from southern Carpathians, Romania. *In* Radoane, M. & Vespremeanu-Stroe, A. (eds.): *Landform Dynamics and Evolution in Romania*, 117–146. Springer Geography, Springer International Publishing, Cham, https://doi.org/10.1007/978-3-319-32589-7_6.

Püspöki, Z., Fogarassy-Pummer, T., Thamó-Bozsó, E., Berényi, B., Cserkész-Nagy, Á., Szappanos, B., Márton, E., Lantos, Z., Nádor, A., Fancsik, T., Stercel, F., Tóth-Makk, Á., McIntosh, R. W., Szőcs, T. & Faragó, E. 2020: High-resolution stratigraphy of a Quaternary fluvial deposit based on magnetic susceptibility variations (Jászság Basin, Hungary). *Boreas 49*, 181–199.

Püspöki, Z., Fogarassy-Pummer, T., Thamó-Bozsó, E., Falus, G., Cserkész-Nagy, Á., Szappanos, B., Márton, E., Lantos, Z., Szilárd, S., Stercel, F., Tóth-Makk, Á., McIntosh, R. W., Szőcs, T., Pálóczy, P. & Fancsik, T. 2021a: High-resolution stratigraphy of Quaternary fluvial deposits in the Makó trough and the Danube-Tisza interfluve based on magnetic susceptibility data (Pannonian Basin, Hungary). *Boreas 50*, 205–223.

Püspöki, Z., Gibbard, P. L., Nádor, A., Thamó-Bozsó, E., Sümegi, P., Fogarassy-Pummer, T., McIntosh, R. W., Lantos, M., Tóth-Makk, Á., Stercel, F., Krassay, Z., Kovács, P., Szőcs, T. & Fancsik, T. 2021b: Fluvial magnetic susceptibility as a proxy on long-term variations of mountain permafrost development in the Alp-Carpathian region. *Boreas 50*, 806–825.

Püspöki, Z., Kovács, I. J., Fancsik, T., Nádor, A., Thamó-Bozsó, E., Tóth-Makk, Á., Udvardi, B., Konya, P., Füri, J., Bendő, Z., Zilahi-Sebess, L., Stercel, F., Gulyás, Á. & McIntosh, R. W. 2016: Magnetic susceptibility as a possible correlation tool in Quaternary alluvial stratigraphy. *Boreas 45*, 861–875.

Ryder, J. M. 1971: The stratigraphy and morphology of para-glacial alluvial fans in south-central British Columbia. *Canadian Journal of Earth Sciences 8*, 279–298.

Smalley, I. J., O'Hara-Dhand, K., Wint, J., Machalett, B., Jary, Z. & Jefferson, I. 2009: Rivers and loess: the significance of long river transportation in the complex event-sequence approach to loess deposit formation. *Quaternary International 198*, 7–18.

Stevens, T., Buylaert, J.-P., Thiel, C., Újvári, G., Yi, S., Murray, A. S., Frechen, M. & Lu, H. 2018: Ice-volume-forced erosion of the Chinese Loess Plateau global Quaternary stratotype site. *Nature Communications 9*, 983, https://doi.org/10.1038/s41467-018-03329-2.

Šujan, M., Braucher, R., Rybár, S., Maglay, J., Nagy, A., Fordinál, K., Šarinová, K., Sýkora, M., Józya, S., Kovač, M. & ASTER Team. 2018: Revealing the late Pliocene to middle Pleistocene alluvial archive in the confluence of the Western Carpathian and Eastern Alpine rivers: 26Al/10Be burial dating from the Danube Basin (Slovakia). *Sedimentary Geology 377*, 131–146.

Sümeghy, B., Kiss, T., Sipos, G. & Tóth, O. 2013: Late Pleistocene – Holocene fluvial landforms of the Maros River alluvial fan. *Földtani Közlöny 143*, 265–278 (in Hungarian).

Sun, J. & Liu, T. 2000: Multiple origins and interpretations of the magnetic susceptibility signal in Chinese wind-blown sediments. *Earth and Planetary Science Letters 180*, 287–296.

Tari, G., Dövényi, P., Dunkl, I., Horváth, F., Lenkey, L., Stefanescu, M., Szafián, P. & Tóth, T. 1999: Lithospheric structure of the Pannonian basin derived from seismic, gravity and geothermal data. *In* Durand, B., Jolivet, L., Horváth, F. & Séranne, M. (eds.): *The Mediterranean Basins: Tertiary Extension within the Alpine Orogen*, 215–250 *Geological Society, London, Special Publication 156*.

Thomson, D. J. 1982: Spectrum estimation and harmonic analysis. *Proceedings of the IEEE 70*, 1055–1096.

Thomson, D. J. 1990: Quadratic-inverse spectrum estimates; applications to paleoclimatology. *Philosophical Transactions of the Royal Society of London. Series A: Physical and Engineering Sciences 332*, 539–597.

Torrence, C. & Compo, G. P. 1998: A practical guide to wavelet analysis. *Bulletin of the American Meteorological Society 79*, 61–78.

van Velzen, A. J. & Dekkers, M. J. 1999: Low-temperature oxidation of magnetite in loess-paleosol sequences: a correction of rock magnetic parameters. *Studia Geophysica et Geodaetica 43*, 357–375.

Ventra, D. & Clarke, L. E. 2018: Geology and geomorphology of alluvial and fluvial fans: current progress and research perspectives. *In* Ventra, D. & Clarke, L. E. (eds.): *Geology and Geomorphology of Alluvial and Fluvial Fans: Terrestrial and Planetary Perspectives*, 1–21 *Geological Society, London, Special Publication 440*.

Walz, F. 2002: The Verwey transition – a topical review. *Journal of Physics: Condensed Matter 14*, R285, https://doi.org/10.1088/0953-8984/14/12/203.

Weedon, G. P. 2003: *Time-Series Analysis and Cyclostratigraphy – Examining Stratigraphic Records of Environmental Cycles*. 259 pp. Cambridge University Press, Cambridge.

Weissmann, G. S., Hartley, A. J., Nichols, G. J., Scuderi, L. A., Olson, M. E., Buehler, H. A. & Massengill, L. C. 2010: Alluvial facies distributions in continental sedimentary basins – distributive fluvial

systems. *In* Davidson, S. K., Leleu, S. & North, C. P. (eds.): *From River to Rock Record*, 327–355. *SEPM Special Publications 97*.
Weissmann, G. S., Hartley, A. J., Scuderi, L. A., Nichols, G. J., Davidson, S. K., Owen, A., Atchley, S. C., Bhattacharyya, P., Chakraborty, T., Ghosh, P., Nordt, L. C., Michel, L. & Tabor, N. J. 2013: Prograding distributive fluvial systems – geomorphic models and ancient examples. *In* Driese, S. G. & Nordt, L. C. (eds.): *New Frontiers in Paleopedology and Terrestrial Paleoclimatology*, 131–147. *SEPM Special Publications 104*.
Weissmann, G. S., Mount, J. F. & Fogg, G. E. 2002: Glacially driven cycles in accumulation space and sequence stratigraphy of stream-dominated alluvial fan, San Joaqiun Valley, California, USA. *Journal of Sedimentary Research 72*, 240–251.
Wórum, G., Koroknai, B., Koroknai, Z., Fekete-Németh, V., Kovács, G. & Tóth, T. 2020: *Young Geological Deformations in Hungary*. Geomega Ltd., Budapest, https://doi.org/10.17632/dnjt9cmj87.1.
Zan, J., Fang, X., Yang, S., Nie, J. & Li, X. 2010: A rock magnetic study of loess from the West Kunlun Mountains. *Journal of Geophysical Research 115*, B10101, https://doi.org/10.1029/2009JB007184.
Zhou, L. P., Oldfield, F., Wintle, A. G., Robinson, S. G. & Wang, J. T. 1990: Partly pedogenetic origin of magnetic variations in Chinese loess. *Nature 346*, 737–739.
Zólyomy, L., Horváth, J. & Sziládi, J. 1985: *A Maros-hordalékkúp vízkutatás 1978–1982 években*. 255 pp. Final report, Hungarian Geological, Geophysical and Mining Datastore.

Supporting Information

Additional Supporting Information to this article is available at http://www.boreas.dk.

Fig. S1. Morphology and seismic sections of the Békés Basin and the Battonya Ridge. A. Pre-Cenozoic basement topography (Haas *et al*. 2014). B. Clinoforms of the Upper Pannonian distributary fluvial system related to the antecedent of the Maros River. C. Kunágota Fault reaching the Quaternary base at the northeastern margin of the Battonya Ridge.

Fig. S2. Complementary data on the investigation of the superparamagnetic fraction. A. Frequency dependent susceptibility (%) vs. low frequency susceptibility plots of the reference boreholes. B. Depth plot of samples taken at 10-cm intervals representing the MP10a magnetic susceptibility maximum in the Kevermes section. C. Temperature dependence of magnetic moment for the Kevermes MP10a magnetic susceptibility maximum in ZFC and FC modes. w is the sample mass and $H = 10$ Oe is the measuring field in both modes and the cooling field in FC mode.

Fig. S3. Depth (A–D) and scatterplots (E–H) of χ_{LF} (logged and measured) and logged sand proxies (gamma ray and resistivity) at Tótkomlós borehole. C and D indicate the accuracy of the sampling for laboratory measurements; E and F indicate the reliability of the proxies; G and H present the relationship between the sand proxies and measured χ_{LF}.